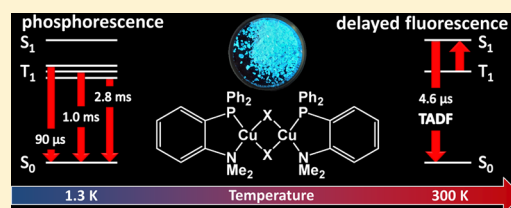


Brightly Blue and Green Emitting Cu(I) Dimers for Singlet Harvesting in OLEDs

Markus J. Leitzl,[†] Fritz-Robert Kühle,[‡] Hermann A. Mayer,[‡] Lars Wesemann,^{*,‡} and Hartmut Yersin^{*,†}[†]Institut für Physikalische und Theoretische Chemie, Universität Regensburg, Universitätsstraße 31, D-93053 Regensburg, Germany[‡]Institut für Anorganische Chemie, Universität Tübingen, Auf der Morgenstelle 18, D-72076 Tübingen, Germany

ABSTRACT: With the chelating aminophosphane ligands Ph₂P-(*o*-C₆H₄)-N(CH₃)₂ (PNMe₂) and Ph₂P-(*o*-C₆H₄)-NC₄H₈ (PNpy), the four halide (Cl, Br, I)-bridged copper coordination compounds [Cu(μ-Cl)(PNMe₂)₂] (1), [Cu(μ-Br)(PNMe₂)₂] (2), [Cu(μ-I)(PNMe₂)₂] (3), and [Cu(μ-I)(PNpy)]₂ (4) were synthesized and structurally characterized. Their photophysical properties were studied in detail. The complexes exhibit strong blue (λ_{max} = 464 (3) and 465 nm (4)) and green (λ_{max} = 506 (1) and 490 nm (2)) luminescence as powders with quantum yields of up to 65% at

decay times as short as 4.1 μs. An investigation of the emission decay behavior between 1.3 and 300 K gives insight into the nature of the emitting states. At temperatures below *T* ≈ 60 K, the decay times of the studied compounds are several hundred microseconds long, which indicates that the emission originates from a triplet state (T₁ state). DFT calculations show that this state is of (metal+halide)-to-ligand charge transfer ³(M+X)LCT character. Investigations at 1.3 K allow us to gain insight into the three triplet substates, in particular, to determine the individual substate decay times being as long as a few milliseconds. The zero-field splittings are smaller than 1 or 2 cm⁻¹. With an analysis of these data, conclusions about the effectiveness of spin–orbit coupling (SOC) can be drawn. Interestingly, the large differences of SOC constants of the halides are not obviously displayed in the triplet state properties. With a temperature increase from *T* ≈ 60 to 300 K, a significant decrease of the emission decay time by almost 2 orders of magnitude is observed, and at ambient temperature, the decay times amount only to ~4–7 μs without a significant reduction of the emission quantum yields. This drastic decrease of the (radiative) decay time is a result of the thermal population of a short-lived singlet state (S₁ state) that lies energetically only a few hundred wavenumbers (460–630 cm⁻¹) higher than the T₁ state. Such an emission mechanism corresponds to a thermally activated delayed fluorescence (TADF). At ambient temperature, almost only a delayed fluorescence (~98%) is observed. Compounds showing this mechanism are highly attractive for applications in OLEDs or LEECs as, in principle, it is possible to harvest all singlet and triplet excitons for the generation of light in the lowest excited singlet state. This effect represents the singlet harvesting mechanism.



1. INTRODUCTION

During the past decades, extensive investigations of organo-transition-metal complexes were carried out. This was driven by the wide range of applications of these materials, especially as emitters in organic light-emitting diodes (OLEDs)^{1–4} and light-emitting electrochemical cells (LEECs).^{5,6} For these applications, third-row transition-metal complexes based on iridium^{7–10} and platinum^{11–16} are well-suited as these central metal ions can induce significant spin–orbit coupling (SOC). Accordingly, fast intersystem crossing (ISC) and effective radiative transitions from the first excited triplet to the ground state become possible.^{17–25} Consequently, attractive emission properties, such as high emission quantum yields of almost 100% and short emission decay times of less than 2 μs, can be achieved.^{18,26,27} In particular, the involvement of the triplet state in the emission process and the fast ISC allow the use of both singlet and triplet excitons for the generation of light in electroluminescent devices and therefore an increase of the efficiency by a factor of 4 compared to that of the usual organic emitters.^{1,2,7,28–30} This mechanism is known as the triplet harvesting effect.^{1,7,28,29} However, with the increasing use of OLEDs, production costs become an important factor. In this

regard, it is desired to find an alternative strategy based on less-expensive materials. Interestingly, copper-based complexes represent a promising emitter class due to their luminescence properties^{31–37} and therefore have recently attracted significant research activities.^{38–53}

Emitter materials applied in electroluminescent devices should exhibit short emission decay times to prevent, for example, saturation effects that would lead to a roll-off of efficiency with increasing current density.^{2,54–56} However, the efficiency of SOC in copper complexes is much smaller than that in Ir or Pt complexes. Obviously, this is in part a consequence of a significantly smaller SOC constant.⁵⁷ In addition, SOC seems to be less efficient than the value of the SOC constant suggests. Therefore, the transition from the triplet excited state to the singlet ground state is strongly spin-forbidden, and this results in emission decay times of several hundred microseconds.^{26,37,41–43,51,53,58,59} Consequently, phos-

Special Issue: Curt Wittig Festschrift

Received: March 26, 2013

Revised: August 22, 2013

phorescent copper complexes are not well applicable if utilized as triplet emitters in OLEDs due to the strong roll-off effects. On the other hand, the energy gap $\Delta E(S_1-T_1)$ between the lowest excited singlet S_1 and triplet T_1 states can be relatively small.^{26,41,43,49,51,53,58,59} Therefore, the singlet state S_1 can be populated thermally at ambient temperature from the energetically lower-lying triplet state T_1 . This mechanism opens a new radiative decay channel to the ground state. The resulting emission represents a thermally activated delayed fluorescence (TADF). As a consequence, the (radiative) emission decay time can be drastically lowered at ambient temperature as compared to the decay time of the triplet state.^{41,49,51,53,58,59} Furthermore, this TADF emission mechanism involves both singlet and triplet states, and therefore, one can exploit singlet and triplet excitons for the generation of light in an electroluminescent device. Because under suitable conditions almost the complete emission stems from the singlet state, this mechanism is called singlet harvesting.^{26,41,51,53,58,59}

In this study, four novel dimeric Cu(I) complexes are presented. The two copper centers in each compound are bridged by two halide atoms (chlorine, bromine, and iodine). As chelating ligands, $\text{Ph}_2\text{P}-(o\text{-C}_6\text{H}_4)\text{-N}(\text{CH}_3)_2$ (PNMe₂) and $\text{Ph}_2\text{P}-(o\text{-C}_6\text{H}_4)\text{-NC}_4\text{H}_8$ (PNpy) are used. We report on the syntheses and structural characterizations of these compounds. Furthermore, a detailed photophysical investigation of all compounds is carried out, focusing on the TADF mechanism and on the lowest excited singlet and triplet state properties. In particular, the triplet state, studied down to $T = 1.3$ K, reflects for the first time details of the effectiveness of SOC in halide-bridged copper compounds.

2. EXPERIMENTAL SECTION

2.1. General Procedures for Synthesis. Starting materials CuCl, CuBr, and CuI were purchased from Aldrich and used as obtained; PNMe₂ was prepared according to a literature method.⁶⁰ For synthesis of PNpy, this literature procedure was slightly modified by replacing phenyldimethylamine with 1-phenylpyrrolidine as the starting material. All chemical preparations were carried out under an argon atmosphere in Schlenk glassware. Solvents used were dried and purified by standard methods and stored under argon.

Preparation of $[\text{Cu}(\mu\text{-X})(\text{PNMe}_2)]_2$ ($X = \text{Cl}, \text{Br}, \text{I}$). To a suspension of CuX (0.19 mmol) in dichloromethane (5 mL), the ligand PNMe₂ (0.19 mmol) was added. The suspension was stirred overnight. The unreacted insoluble educts were filtered off, and after slow diffusion of *n*-hexane into the dichloromethane phase at +4 °C, the product $[\text{Cu}(\mu\text{-X})(\text{PNMe}_2)]_2$ was obtained as colorless crystals.

$[\text{Cu}(\mu\text{-Cl})(\text{PNMe}_2)]_2$ (1). Yield: 59 mg (77%). ¹H NMR (CD₂Cl₂): δ 2.77 (s, 12H, NMe), 7.22–7.52 (m, 28H, Ar). ³¹P {¹H} NMR (CD₂Cl₂): δ –20.8 (s). Anal. Calcd for C₄₀H₄₀Cl₂Cu₂N₂P₂ (808.72): C, 59.41; H, 4.99; N, 3.46. Found: C, 58.99; H, 4.90; N, 3.35.

$[\text{Cu}(\mu\text{-Br})(\text{PNMe}_2)]_2$ (2). Yield: 64 mg (75%). ¹H NMR (CD₂Cl₂): δ 2.65 (s, 12H, NMe), 7.09–7.44 (m, 28H, Ar). ³¹P {¹H} NMR (CD₂Cl₂): δ –24.6 (s). Anal. Calcd for C₄₀H₄₀Br₂Cu₂N₂P₂ (897.62): C, 53.52; H, 4.49; N, 3.12. Found: C, 53.45; H, 4.59; N, 3.09.

$[\text{Cu}(\mu\text{-I})(\text{PNMe}_2)]_2$ (3). Yield: 74 mg (79%). ¹H NMR (CD₂Cl₂): δ 2.64 (s, 12H, NMe), 7.07–7.45 (m, 28H, Ar). ³¹P {¹H} NMR (CD₂Cl₂): δ –27.3 (s). Anal. Calcd for C₄₀H₄₀I₂Cu₂N₂P₂ (991.62): C, 48.45; H, 4.07; N, 2.83. Found: C, 48.50; H, 4.16; N, 2.83.

Preparation of $[\text{Cu}(\mu\text{-I})(\text{PNpy})]_2$. The same procedure as that described above for $[\text{Cu}(\mu\text{-X})(\text{PNMe}_2)]_2$ was applied to obtain $[\text{Cu}(\mu\text{-I})(\text{PNpy})]_2$ from CuI (0.19 mmol) and PNpy (0.19 mmol).

$[\text{Cu}(\mu\text{-I})(\text{PNpy})]_2$ (4). Yield: 75 mg (76%). ¹H NMR (CD₂Cl₂): δ 1.94 (br, 8H, NCH₂CH₂), 3.17 (br, 8H, NCH₂CH₂), 7.08–7.60 (m, 28H, Ar). ³¹P {¹H} NMR (CD₂Cl₂): δ –24.9 (br). Anal. Calcd for C₄₄H₄₄I₂Cu₂N₂P₂ (1043.70): C, 50.64; H, 4.25; N, 2.68. Found: C, 50.25; H, 4.00; N, 2.64.

2.2. Instrumentation and Methods. NMR spectra were recorded with a Bruker DRX-250 NMR spectrometer equipped with a 5 mm BBO probe operating at 250.13 (¹H) and 101.25 MHz (³¹P), respectively. Chemical shifts are reported in ppm relative to external 1% TMS in chloroform (¹H) and 85% aq H₃PO₄ (³¹P) using the chemical shift of the deuterated solvent ²H resonance frequency for calibration. Elemental analyses were carried out with an elemental analyzer Vario EL.

X-ray data of the compounds were collected with a Stoe IPDS 2T diffractometer and corrected for Lorentz and polarization effects and absorption by air. The programs used in this work were Stoe's X-Area and WinGX suite of programs including SHELXS and SHELXL for structure solution and refinement.^{61,62} Numerical absorption correction based on crystal-shape optimization was applied with Stoe's X-Red and X-Shape.^{61,63}

Luminescence and excitation spectra were recorded using a Fluorolog 3-22 (Horiba Jobin Yvon) spectrophotometer. Emission decay times were measured with a cooled photomultiplier (RCA C7164R) combined with a FAST ComTec multichannel scaler PCI card with a time resolution of 250 ps. A pulsed Nd:YAG laser ($\lambda_{\text{exc}} = 355$ nm, pulse width < 8 ns) was used as the excitation light source. Temperature-dependent measurements between 1.3 and 300 K of emission decay times and spectra were performed using a helium cryostat (Cryovac Konti Cryostat IT) with controlled helium gas flow and heating. For absolute measurements of photoluminescence quantum yields at ambient temperature and at 77 K, a Hamamatsu Photonics (C9920-02) system was used. DFT and TDDFT calculations were performed with the NWChem 6.1 software package⁶⁴ using the hybrid functional B3LYP.⁶⁵ For all calculations, the basis sets 6-31G*^{66–69} (for H, C, N, P), m-631G*⁷⁰ (for Cu), and LANL2DZ with an effective core potential (ECP)^{71–74} (for Cl, Br and I) were applied. As the starting input for the geometry optimizations, data retrieved from crystal structure measurements were used. The convergence criteria were left at the standard settings, and no symmetry constraints were applied. The results (Figure 4) were visualized using Chemcraft 1.6.

3. RESULTS AND DISCUSSION

3.1. Syntheses and Crystal Structures. The studied complexes were prepared by reacting equimolar amounts of the respective copper halide with the respective chelating ligand (Figure 1). Single crystals of the copper coordination compounds were obtained after slow diffusion of *n*-hexane into a dichloromethane solution. The chemical structures of the resulting compounds were identified by ¹H and ³¹P NMR as well as by X-ray structure analysis. In Table 1, the crystallographic data of substances 1–4 are summarized. The respective ORTEP representations are shown in Figure 2, and selected atomic distances and angles are given in Table 2. Two different coordination structures were found for the investigated

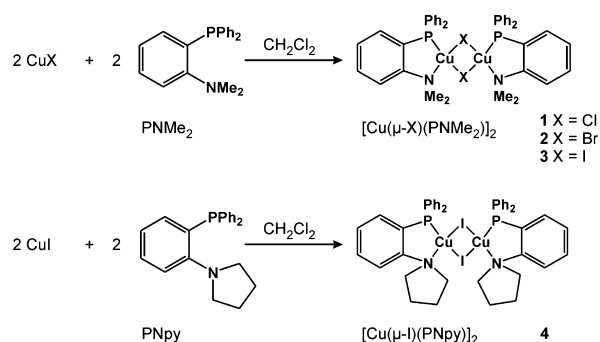


Figure 1. Reaction scheme for the compounds $[\text{Cu}(\mu\text{-Cl})(\text{PNMe}_2)_2]_2$ (1), $[\text{Cu}(\mu\text{-Br})(\text{PNMe}_2)_2]_2$ (2), $[\text{Cu}(\mu\text{-I})(\text{PNMe}_2)_2]_2$ (3), and $[\text{Cu}(\mu\text{-I})(\text{PNpy})_2]_2$ (4). Me and Ph represent methyl and phenyl groups, respectively.

substances. In compound 1, the copper and halide atoms are located in one plane, in contrast to compounds 2–4 where these atoms include distinct dihedral angles Br1–Cu2–Cu1–Br2 of 128.2° (2), I1–Cu2–Cu1–I2 of 132.7° (3), and I1–Cu2–Cu1–I2 of 139.6° (4). Additionally, the orientation of the organic ligands relative to each other differs between these two types of structures. An analysis of the interatomic distances of the substances containing the PNMe₂ ligand (compounds 1–3) reveals that the lengths of the copper halide bonds (Cu1–X1) increase from 1 (2.369 Å) to 2 (2.418 Å) to 3 (2.582 Å). This

trend is also reflected in the other Cu–X bonds (Cu1–X2, Cu2–X1, and Cu2–X2). Furthermore, a slightly larger Cu1–Cu2 distance is found for 3 (2.574 Å) than that for 2 (2.559 Å). Replacing the PNMe₂ ligand (compound 3) by PNpy (compound 4) leads to a significant increase of the Cu–Cu distance to 2.688 Å due to the increased sterical demand of the PNpy ligand. However, compound 1 exhibits the largest Cu1–Cu2 distance (2.983 Å), which is a result of the planar structure of the copper halide core of this molecule. Thus, large variations of the Cu–Cu distances ranging from about 2.56 to 2.98 Å are observed for the studied complexes 1–4. Similarly large variations occur also for other halide-bridged dinuclear copper complexes.^{38,75–80} For completeness, it is remarked that the calculated intramolecular distances and angles, as summarized in Table 2, fit fairly well to those determined experimentally. This accordance gives us the confidence that also the calculated electronic structures are adequately described, at least with respect to the discussed trends of a significant charge transfer (CT) upon excitation from the occupied to the unoccupied MOs and the shifts of transition energies in this series.

3.2. Spectroscopic Introduction. The studied compounds show intense blue (3, 4) and green (1, 2) luminescence under UV excitation. At first, we will focus on photophysical properties of compound 3. The measurements were performed with powder samples due to the limited chemical stability in solution (e.g., toluene). A justification for this approach is given

Table 1. Crystallographic Data for the Cu(I) Dimers 1–4

compound	1 $[\text{Cu}(\mu\text{-Cl})(\text{PNMe}_2)_2]_2$	2 $[\text{Cu}(\mu\text{-Br})(\text{PNMe}_2)_2]_2$	3 $[\text{Cu}(\mu\text{-I})(\text{PNMe}_2)_2]_2$	4 $[\text{Cu}(\mu\text{-I})(\text{PNpy})_2]_2$
empirical formula	$\text{C}_{40}\text{H}_{40}\text{Cl}_2\text{Cu}_2\text{N}_2\text{P}_2$	$\text{C}_{40}\text{H}_{40}\text{Br}_2\text{Cu}_2\text{N}_2\text{P}_2$	$\text{C}_{40}\text{H}_{40}\text{Cu}_2\text{I}_2\text{N}_2\text{P}_2$	$\text{C}_{44}\text{H}_{44}\text{Cu}_2\text{I}_2\text{N}_2\text{P}_2$
M [g mol ^{−1}]	808.68	897.58	991.58	1043.63
wavelength [Å]	0.71073	0.71073	0.71073	0.71073
temperature [K]	173(2)	173(2)	173(2)	173(2)
crystal system	triclinic	monoclinic	monoclinic	monoclinic
space group	$P\bar{1}$	$P 2_1/n$	$P 2_1/c$	$C2/c$
Z	1	4	4	4
a [Å]	9.373(1)	17.793(1)	18.158(1)	24.867(2)
b [Å]	10.050(1)	9.861(1)	9.941(1)	10.153(1)
c [Å]	11.436(1)	23.329(1)	23.312(1)	23.722(2)
α [°]	78.77(1)			
β [°]	70.64(1)	112.34(1)		137.25(1)
γ [°]	65.41(1)		110.50(1)	
volume [Å ³]	922.2(2)	3786.0(1)	3941.7(4)	4065.8(5)
density ρ_{calc} [g/cm ³]	1.456	1.575	1.671	1.705
abs. coeff. μ [mm ^{−1}]	1.416	3.350	2.757	2.677
$F(000)$	416	1808	1952	2064
crystal size [mm ³]	$0.32 \times 0.22 \times 0.14$	$0.21 \times 0.19 \times 0.19$	$0.22 \times 0.18 \times 0.15$	$0.20 \times 0.20 \times 0.20$
theta range [°]	2.64–29.13	3.08–29.20	2.47–29.16	5.28–29.20
limiting indices h, k, l	−12/12, −13/13, −15/15	−24/24, −13/13, −31/31	−24/24, −13/13, −31/31	−34/34, −13/13, −32/32
reflections collected	17451	68614	72402	36406
ind. refl./[$R(\text{int})$]	4958/[0.0673]	10197 [0.0862]	10606 [0.1025]	5434 [0.1073]
completeness	99.8%	99.5%	99.6%	98.8
absorption correction	numerical	numerical	numerical	numerical
max., min transmission	0.8567, 0.6787	0.6112, 0.5132	0.7340, 0.5807	0.6805, 0.5822
restraints/parameters	0/217	0/433	0/433	0/235
R_1, wR_2 [$I > 2\sigma(I)$]	0.0389, 0.0948	0.0551, 0.1030	0.0403, 0.0846	0.0502, 0.1228
R_1, wR_2 all data	0.0427, 0.0967	0.0707, 0.1078	0.0475, 0.0864	0.0562, 0.1262
goodness-of-fit on F^2	1.088	1.255	1.398	1.150
largest diff. peak, hole [e^- Å ^{−3}]	0.780, −0.827	0.811 −0.819	0.758, −1.111	1.577, −2.238
CCDC number	929959	929960	929958	929961

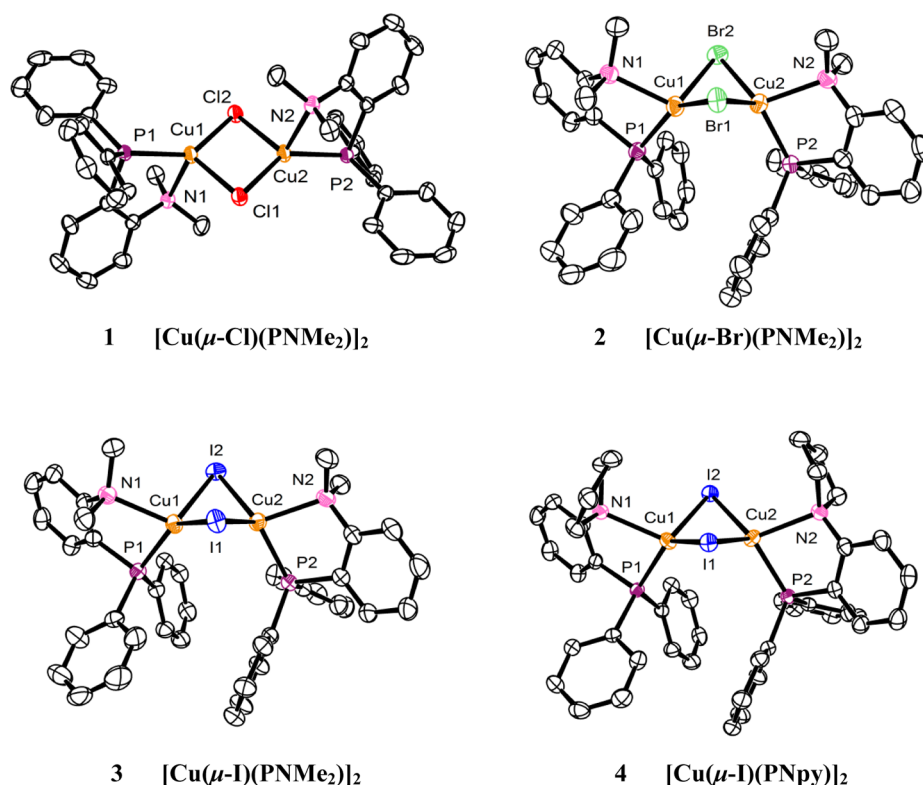


Figure 2. ORTEP representation (50% ellipsoids) of 1–4 from X-ray structure determinations. Hydrogen atoms are not displayed for clarity.

Table 2. Selected Interatomic Distances and Angles of the Copper Complexes 1–4 As Obtained from X-ray Analyses^a

compound	1	2	3	3 (calcd)	4
Cu2–X1 [Å]	2.283(1)	2.499(1)	2.634(1)	2.674	2.646(1)
Cu1–X1 [Å]	2.369(1)	2.418(1)	2.582(1)	2.720	2.597(1)
Cu1–X2 [Å]	2.283(1)	2.542(1)	2.666(1)	2.673	2.646(1)
Cu2–X2 [Å]	2.369(1)	2.417(1)	2.590(1)	2.720	2.597(1)
Cu1–Cu2 [Å]	2.983(1)	2.559(1)	2.574(1)	2.639	2.688(1)
Cu1–N1 [Å]	2.305(2)	2.248(3)	2.250(3)	2.412	2.328(3)
Cu2–N2 [Å]	2.305(2)	2.231(3)	2.232(3)	2.410	2.328(3)
Cu1–P1 [Å]	2.175(1)	2.190(1)	2.210(1)	2.265	2.222(1)
Cu2–P2 [Å]	2.175(1)	2.189(1)	2.213(1)	2.265	2.222(1)
Cu1–X1–Cu2 [°]	79.8(1)	62.7(2)	59.1(1)	58.6	61.7(2)
Cu1–X2–Cu2 [°]	79.8(1)	62.1(2)	58.6(1)	58.6	61.7(2)
X1–Cu1–X2 [°]	100.2(1)	100.0(1)	105.5(2)	108.9	107.4(1)
X1–Cu2–X2 [°]	100.2(1)	101.3(1)	106.2(2)	108.9	107.4(1)
N1–Cu1–P1 [°]	84.4(1)	83.6(1)	83.3(1)	80.7	82.4(1)
N2–Cu2–P2 [°]	84.4(1)	85.0(1)	84.2(1)	80.7	82.4(1)
X1–Cu2–Cu1–X2 [°]	0	128.2(1)	132.7(1)	137.8	139.6(1)

^aIn addition, for compound 3, data obtained from a DFT calculation are displayed. The calculated results refer to a ground-state geometry optimization.

below. Figure 3 shows emission and excitation spectra measured at ambient and liquid nitrogen temperatures, respectively. With temperature variation, distinct changes of the emission properties are observed. At $T = 77$ K, the emission maximum lies at $\lambda_{\text{max}}(77 \text{ K}) = 471$ nm (50% high-energy flank at 443 nm), the decay time amounts to $\tau(77 \text{ K}) = 270 \mu\text{s}$, and the quantum yield $\Phi_{\text{PL}}(77 \text{ K})$ is as high as almost 100%. According to this relatively long decay time and due to the detailed investigations at lower temperatures ($T = 1.3$ K, compare section 3.4), we assign the state emitting at low temperature as the triplet state T_1 with a singlet ground state S_0 . With a temperature increase to $T = 300$ K, a slight blue shift of

the emission to $\lambda_{\text{max}}(300 \text{ K}) = 464$ nm (50% high-energy flank at 433 nm) and a drastic decrease of the emission decay time to $\tau(300 \text{ K}) = 4.6 \mu\text{s}$ are observed, while the quantum yield decreases only slightly to $\Phi_{\text{PL}}(300 \text{ K}) = 65\%$. A comparison of the decay times and quantum yields at the different temperatures reveals an interesting behavior. According to $k_r = \Phi_{\text{PL}}\tau^{-1}$, the corresponding radiative rates k_r can be determined. The rate increases from $k_r(77 \text{ K}) = 3.7 \times 10^3 \text{ s}^{-1}$ to $k_r(300 \text{ K}) = 1.4 \times 10^5 \text{ s}^{-1}$, that is, by more than a factor of 40. Obviously, with a temperature increase from 77 to 300 K, a different emission process is thermally activated. In the

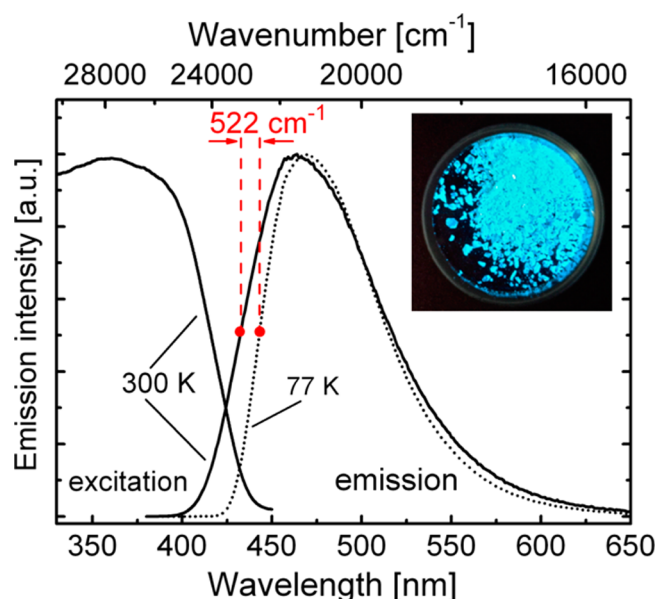


Figure 3. Emission and excitation spectra of compound **3** (powder) at ambient temperature (solid line) and 77 K (dotted line). The emission spectra were recorded under excitation at $\lambda_{\text{exc}} = 360$ nm, and the excitation spectra were detected at $\lambda_{\text{det}} = 470$ nm. The inset shows a photo of the powder sample of compound **3** excited at 365 nm.

following section, we will assign this behavior to be a consequence of a TADF.

Interestingly, concentration quenching in the powder samples, being usually connected with energy-transfer processes between adjacent molecules,⁸¹ does not seem to be of importance for the studied complexes. This is indicated by the observed high emission quantum yields and the monoexponential decay behavior in the whole temperature range from ~20 to 300 K. This behavior can be rationalized by assuming that, even in the solid phase, the excited states undergo (at least) a small geometry distortion^{43,82–86} that leads to a lowering of the excited-state energy. As a consequence, the energy cannot be transferred from an excited to an adjacent nonexcited emitter molecule as the resonance condition for this process is not fulfilled. A related self-trapping behavior has been discussed in ref 87. In addition, it is remarked that in powders of several other Cu(I) complexes, such a self-trapping effect does not occur. In particular, this is observed for compounds that exhibit low-lying ligand-centered transitions of $\pi\pi^*$ character with no significant geometry change upon excitation.

The type of the electronic transition and the characters of the involved orbitals can be elucidated by carrying out DFT and TDDFT calculations. Applying the methods described in section 2, HOMO and LUMO contour curves are obtained for the (optimized) ground-state geometry (Figure 4). The pronounced spatial separation of these frontier orbitals indicates that the HOMO–LUMO transition possesses significant CT character. More specifically, with an excitation, charge is transferred from the d orbitals of the copper and the p orbitals of the iodine atoms to the unoccupied orbitals. The latter ones are mainly located on the PNMe₂ ligands. Therefore, this transition can be assigned to be of (metal+halide)-to-ligand charge transfer ((M+X)LCT) character.

TDDFT calculations give an insight into the molecular orbital contributions to the electronic energy states. For example, the HOMO–LUMO transition contributes to the

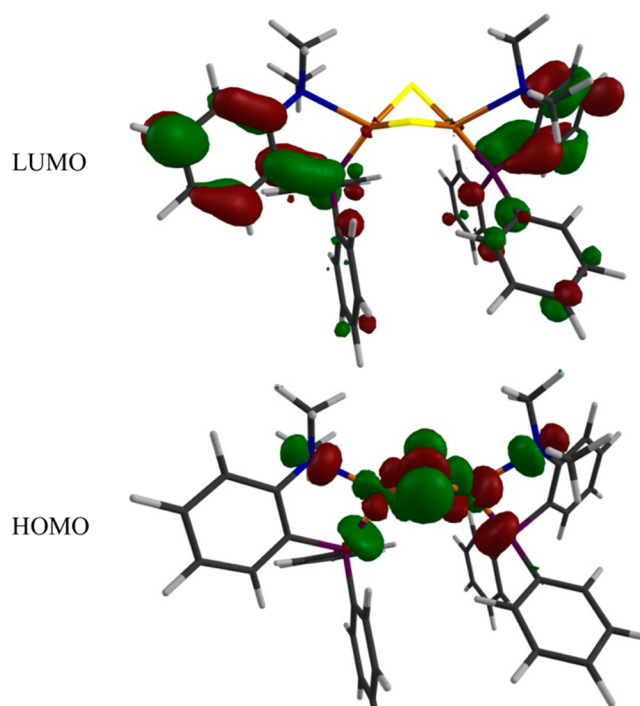


Figure 4. HOMO and LUMO of compound **3** for the ground state S_0 geometry in the gas phase. The basis sets used were 6-31G* (H, C, N, P), m6-31G* (Cu), and LANL2DZ with an ECP (I). B3LYP was used as the functional.

lowest singlet and triplet state by ~70 and ~50%, respectively. A further significant contribution comes from the HOMO–1 to LUMO+1 transition, which amounts ~25% for the singlet and ~30% for the triplet state. All contributing occupied orbitals (HOMO, HOMO–1) are located on copper and on iodine, whereas all contributing unoccupied orbitals (LUMO, LUMO+1) are located on the ligands. This means that the lowest excited states represent $^1,3(M+X)LCT$ states.

A significant CT character is usually connected with relatively broad and unstructured spectra. Indeed, the experimentally determined emission spectra are broad even at low temperatures and thus are in agreement with this prediction (Figure 3).

In Figure 5, ambient temperature emission spectra are reproduced for the four investigated compounds. Interestingly, for substances **3** and **4**, which both contain iodine as the bridging halide, no significant differences in the emission energy and shape of the spectrum are observed, although the Cu–Cu separations differ by more than 1 Å. On the other hand, a remarkable blue shift of the emission energies occurs in the series from **1** to **3**. The emission peak maxima lie at 506 (Cl), 490 (Br), and 464 nm (I). A similar shift is also observed for the emission maxima at 77 K (mainly representing triplet state T_1 emissions). DFT calculations show that the energy shift is essentially caused by a stabilization of the HOMO in the series from Cl, Br, and I, whereas the LUMO remains almost at the same energy, as is displayed for the optimized triplet state geometry. For completeness, it is remarked that this trend is in agreement with the effect that one would expect from a decrease of the ligand field strength in the series of $Cl^- > Br^- > I^-$.⁵¹

In Table 3, photophysical data for the investigated compounds are summarized. The emission quantum yields at

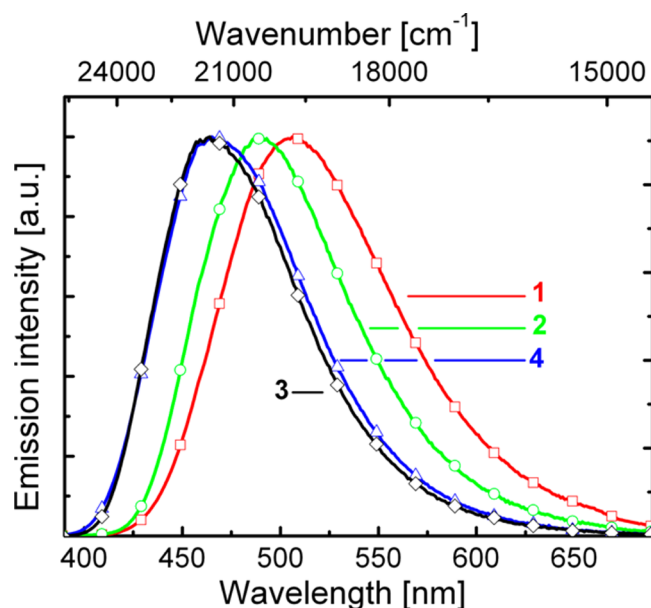
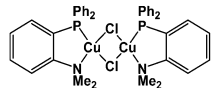
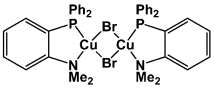
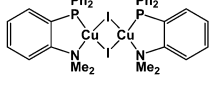
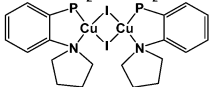


Figure 5. Emission spectra of substances $[\text{Cu}(\mu\text{-Cl})(\text{PNMe}_2)_2]_2$ (1), $[\text{Cu}(\mu\text{-Br})(\text{PNMe}_2)_2]_2$ (2), $[\text{Cu}(\mu\text{-I})(\text{PNMe}_2)_2]_2$ (3), and $[\text{Cu}(\mu\text{-I})(\text{PNpy})_2]_2$ (4) measured as powders at ambient temperature ($\lambda_{\text{exc}} = 360 \text{ nm}$).

Table 3. Photophysical Properties of the Powders of the Compounds 1–4 Measured at Ambient and Liquid Nitrogen Temperature^a

Compound	Temp. [K]	λ_{max} [nm]	τ [μs]	Φ_{PL} [%]	k_r [s^{-1}]
	300	506	6.6	45	$6.8 \cdot 10^4$
	77	513	220	~100	$4.5 \cdot 10^3$
	300	490	4.1	65	$1.6 \cdot 10^5$
	77	498	930	~100	$1.1 \cdot 10^3$
	300	464	4.6	65	$1.4 \cdot 10^5$
	77	471	270	~100	$3.7 \cdot 10^3$
	300	465	5.6	65	$1.2 \cdot 10^5$
	77	465	250	~100	$4.0 \cdot 10^3$

^a λ_{max} is the peak wavelength of the emission spectrum, τ the emission decay time, Φ_{PL} the photoluminescence quantum yield, and k_r the radiative decay rate.

$T = 300 \text{ K}$ are equal within limits of experimental error for the compounds 2–4 ($\Phi_{\text{PL}} = 65\%$), whereas compound 1 exhibits a lower value of $\Phi_{\text{PL}} = 45\%$. However, the chemical structure of compound 1 differs from those of the other substances in the position of the copper and halide atoms relative to each other as well as in the orientations of the ligands (compare Figure 2). Therefore, a direct comparison of the photophysical properties of these two structure types is difficult. Presumably, the lower quantum yield of 1 is related to a more flexible structure with respect to excited-state geometry changes, which result in an increase of nonradiative deactivation processes. Indeed, the

much larger Cu–Cu separation found for 1 as compared to that for 2–4 (Table 2) supports this model. Furthermore, a comparison of the Φ_{PL} values at ambient and nitrogen temperatures reveals that an increase of the quantum yields occurs with decreasing temperature. A behavior like this is not unusual and is related to a decrease of nonradiative deactivations on cooling.

The emission decay times measured at 300 K for the four compounds do not differ significantly. They lie between about 4 and 7 μs . These values are dominated by the energy separations between the excited singlet (S_1) and triplet (T_1) states. A detailed discussion is found in the next section. However, at 77 K, the emission decay times of the different compounds deviate significantly and range from 220 to 930 μs . These differences are related to the SOC being differently effective in the four compounds. Corresponding effects are discussed in more detail in section 3.4.

Similar as already described above for 3, compounds 1 and 2 exhibit a red shift of the emission when cooled to 77 K. (For compound 4, this red shift is only displayed at the high-energy flanks of the emission spectra.) The red shift is accompanied by the drastic increase of the emission decay time but is not paralleled by an increase of the emission quantum yield. Obviously, cooling results in a drastic lowering of the radiative rates. This effect is most pronounced for compound 2 for which the radiative rate decreases by a factor of almost 150. The decrease of the radiative rates along with a red shift of the emission with decreasing temperature indicates that all studied materials show the effect of TADF at ambient temperature. In the following section, this mechanism will be discussed in more detail.

3.3. TADF. A deeper understanding of the emission properties is obtained by studying the decay time as a function of temperature in the range between 30 and 300 K. In the entire temperature range, the decay is monoexponential. The result is depicted in Figure 6 for the representative example 3.

For this compound, the emission decay time is almost constant in the temperature range between about 20 and 60 K,

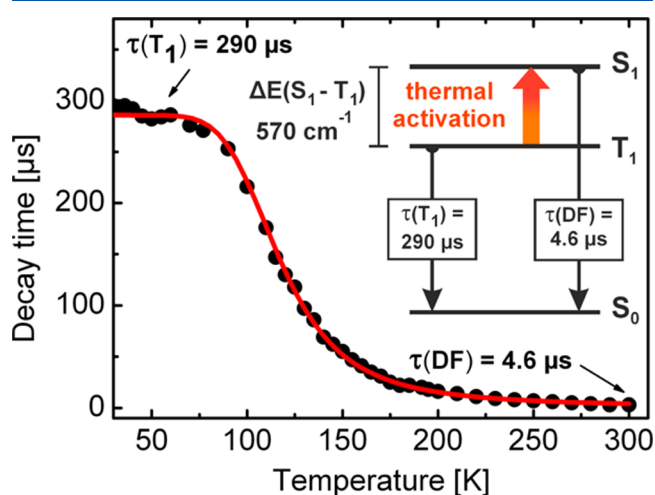


Figure 6. Temperature dependence of the emission decay time of substance 3 as a powder. The solid red line represents the fit of the experimental data according to eq 1. The compounds were excited with a pulsed laser at a wavelength of 355 nm (pulse width of $\sim 8 \text{ ns}$). The emission was detected at the maximum of each emission spectrum.

and one observes a plateau with $\tau \approx 290 \mu\text{s}$. Accordingly, this emission is assigned as phosphorescence from the triplet state T_1 to the ground state S_0 . Further evidence for the triplet character is given in the next section. According to the discussion presented above, this triplet is of $^3(\text{M}+\text{X})\text{LCT}$ parentage. With temperature increase, a strong reduction of the emission decay time is observed. This is attributed to a thermal activation of a higher-lying electronic state, which carries significantly more allowance of the transition to the ground state than the T_1 state. Therefore, the corresponding state is assigned as the lowest excited singlet state S_1 being of $^1(\text{M}+\text{X})\text{LCT}$ character. This effect represents a TADF. At temperatures above $T \approx 120 \text{ K}$, the contribution of the singlet state to the emission dominates (see below). For thermally equilibrated states, the emission decay time of the two excited state system can be expressed as a function of the temperature according to eq 1, which represents an adaption from treatments found in the literature.^{18,59,88,89} (For this treatment, it has to be taken into account that the T_1 state consists of three substates (see also below).)

$$\tau(T) = \frac{3 + \exp\left[-\frac{\Delta E(S_1-T_1)}{k_B T}\right]}{\frac{3}{\tau(T_1)} + \frac{1}{\tau(S_1)} \exp\left[-\frac{\Delta E(S_1-T_1)}{k_B T}\right]} \quad (1)$$

In this equation, k_B represents the Boltzmann constant, and $\tau(S_1)$ and $\tau(T_1)$ are the emission decay times of the singlet state S_1 and the triplet state T_1 , respectively, in the absence of thermalization. $\Delta E(S_1-T_1)$ is the energy separation (activation energy) between these two states. Because in the temperature range investigated a single-exponential decay behavior was found, it can be concluded that in fact a fast thermalization between the two excited states occurs, and thus, eq 1 can be applied. Fitting this equation to the measured decay time data allows us to determine the decay time of the prompt fluorescence to $\tau(S_1) = 90 \text{ ns}$, the decay time of the phosphorescence to $\tau(T_1) = 290 \mu\text{s}$ (corresponding to the plateau seen in Figure 6), and the energy separation between the two states to $\Delta E(S_1-T_1) = 570 \text{ cm}^{-1}$. The short decay time of 90 ns determined for the thermally activated state substantiates its singlet character. Thus, the measured emission decay time at $T = 300 \text{ K}$ of $\tau(\text{DF}) = 4.6 \mu\text{s}$ represents an $S_1 \rightarrow S_0$ fluorescence, which, however, because it is fed by the long-lived triplet state reservoir, represents a delayed fluorescence. It is remarked that despite this short decay time of the singlet state, no spontaneous fluorescence is directly observed. This indicates that the ISC is much faster than the emission processes.

The energy separation between the singlet S_1 and the triplet T_1 states with $\Delta E(S_1-T_1) = 570 \text{ cm}^{-1}$ is very small as compared to other organo-transition-metal complexes, such as $\text{Pd}(\text{II})$ or $\text{Pt}(\text{II})$ compounds with $\Delta E(S_1-T_1)$ values of several 10^3 cm^{-1} .^{90,91} This behavior of the $\text{Cu}(\text{I})$ compound is ascribed to be a consequence of the distinct spatial separation of the occupied and unoccupied frontier orbitals, in particular, of the HOMO and LUMO, which leads to a small electron exchange interaction and therefore to a small singlet–triplet energy separation (e.g., compare ref 92).

An alternative approach to determine the energy separation $\Delta E(S_1-T_1)$ is to compare the emission spectra at $T = 77 \text{ K}$ (almost pure triplet emission) and $T = 300 \text{ K}$ (almost pure singlet emission). The energy separation of these spectra, taken at the high-energy flank at 50% of the maximum intensity,

amounts to $\Delta E(S_1-T_1) = 522 \text{ cm}^{-1}$ and thus matches well to the value found from the fit procedure. The spectral blue shift of the emission toward higher temperatures substantiates further that a higher electronic state is thermally populated. This strongly indicates that TADF is the dominant emission mechanism of this compound at high temperatures.

For the compounds **1**, **2**, and **4**, similar investigations with respect to the temperature dependence of the decay times have been carried out. The resulting data are summarized in Table 4.

Table 4. Overview of the Properties of the First Excited Singlet and Triplet States of the Investigated Substances

compound	1	2	3	4
$\Delta E(S_1-T_1)^a$ [cm^{-1}]	460	510	570	630
$\tau(T_1)^a$ [μs]	250	1200	290	250
$\tau(S_1)^a$ [ns]	210	110	90	100
$\tau(\text{DF})^b$ [μs]	6.6	4.1	4.6	5.6

^aFrom the fit. ^bMeasured at $T = 300 \text{ K}$.

An analysis of these data allows us to come to a better understanding of the emission process. All compounds exhibit small values for the singlet–triplet splitting $\Delta E(S_1-T_1)$ ranging from 460 to 630 cm^{-1} and therefore show pronounced TADF at ambient temperature. For the triplet decay times $\tau(T_1)$, distinctly different values are found. A more detailed discussion of this property is presented in the following section. For the decay time (fit data) of the singlet state $\tau(S_1)$, values amounting to 90–210 ns are determined. Hereby, compounds **2**, **3**, and **4** show very similar decay times of 90–110 ns, while compound **1** exhibits by a factor of about two longer decay time of 210 ns compared to the other substances. This can be a consequence of a more distinct CT that is connected with a smaller transition dipole moment of the corresponding transition, leading to a weaker allowedness. Moreover, the more pronounced CT character also should result in a smaller value for $\Delta E(S_1-T_1)$ as the wave functions' overlap is smaller, which results in a smaller exchange interaction. Indeed, complex **1** shows the smallest $\Delta E(S_1-T_1)$ value of the investigated substances. The more distinct CT character of the $S_1 \rightarrow S_0$ fluorescence in compound **1** could be a result of the different molecular geometry of compound **1** compared to the other substances (compare Figure 2). At ambient temperature, the decay times of the delayed fluorescence $\tau(\text{DF})$ range from 4.1 to 6.6 μs . These values are governed by the singlet decay times $\tau(S_1)$ and the singlet–triplet splittings $\Delta E(S_1-T_1)$ of the respective compounds. The influence of the triplet lifetime $\tau(T_1)$ on $\tau(\text{DF})$ can be neglected for these compounds at ambient temperature. Interestingly, compound **1**, which exhibits the smallest $\Delta E(S_1-T_1)$ value, also shows the longest delayed fluorescence decay time of $\tau(\text{DF}) = 6.6 \mu\text{s}$. This is a consequence of the relatively long singlet decay time of $\tau(S_1) = 210 \text{ ns}$.

It is illustrative to visualize the percentage of the intensity originating from the singlet $I(S_1)$ and from the triplet state $I(T_1)$ relative to the total intensity I_{tot} in dependence of the temperature. $I(S_1)$ is proportional to the population of the singlet state $N(S_1)$ and to the radiative rate constant $k_r(S_1)$

$$I(S_1) = ak_r(S_1)N(S_1) \quad (2)$$

In the same way, $I(T_1)$ is given by

$$I(T_1) = ak_r(T_1)N(T_1) \quad (3)$$

α is a proportionality constant that is equal in both equations. The radiative rates $k_r(S_1)$ and $k_r(T_1)$ can be expressed in terms of the quantum yields and the emission decay times according to $k_r = \Phi_{PL}\tau^{-1}$. For this rough estimate, we further assume that the quantum yields $\Phi_{PL}(S_1)$ and $\Phi_{PL}(T_1)$ do not depend on the temperature. With this, $I_{tot} = I(S_1) + I(T_1)$, and assuming that the populations of both states follow a Boltzmann distribution (fast equilibration), one obtains

$$\frac{I(T_1)}{I_{tot}} = \left[1 + \frac{k_r(S_1)g(S_1)}{k_r(T_1)g(T_1)} e^{-\Delta E(S_1-T_1)/k_B T} \right]^{-1} \\ = \left[1 + \frac{\Phi_{PL}(S_1)\tau(T_1)}{3\Phi_{PL}(T_1)\tau(S_1)} e^{-\Delta E(S_1-T_1)/k_B T} \right]^{-1} \quad (4)$$

$g(S_1) = 1$ and $g(T_1) = 3$ are the degeneracy factors for the singlet and the triplet states respectively. Using $I(T_1) = I_{tot} - I(S_1)$ leads to

$$\frac{I(S_1)}{I_{tot}} = 1 - \left[1 + \frac{\Phi_{PL}(S_1)\tau(T_1)}{3\Phi_{PL}(T_1)\tau(S_1)} e^{-\Delta E(S_1-T_1)/k_B T} \right]^{-1} \quad (5)$$

Applying eq 4 and 5 and using the fit parameters as determined for compound 3 ($\Delta E(S_1-T_1) = 570 \text{ cm}^{-1}$, $\tau(S_1) = 90 \text{ ns}$, $\tau(T_1) = 290 \mu\text{s}$, $\Phi_{PL}(S_1) = 0.65$, and $\Phi_{PL}(T_1) = 1$), the plots shown in Figure 7 are obtained. At low temperature ($T < 60 \text{ K}$), only a

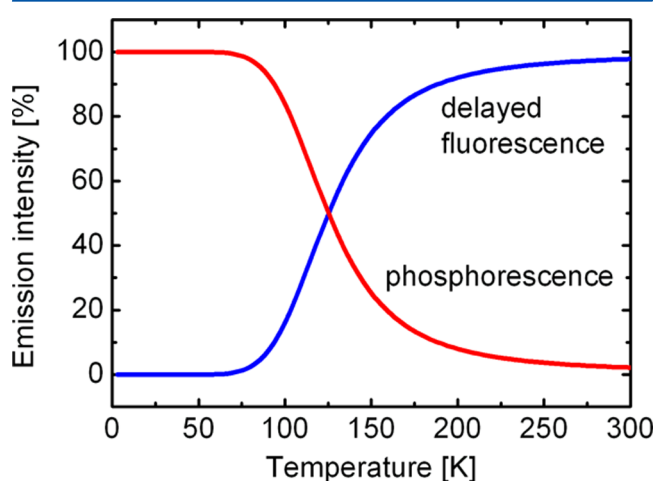


Figure 7. The emission intensities stemming from the singlet state S_1 (delayed fluorescence) and the triplet state T_1 (phosphorescence), normalized to the total intensity $I_{tot} = I(S_1) + I(T_1)$ in dependence of temperature according to eqs 4 and 5. The parameters used are the ones found for compound 3 ($\Delta E(S_1-T_1) = 570 \text{ cm}^{-1}$, $\tau(T_1) = 290 \mu\text{s}$, $\tau(S_1) = 90 \text{ ns}$, $\Phi_{PL}(S_1) = 0.65$, and $\Phi_{PL}(T_1) = 1$).

T_1 phosphorescence occurs. With a temperature increase, the intensity contributed from the T_1 state decreases, while the intensity stemming from the S_1 state increases. At $T = 300 \text{ K}$, almost all intensity (98%) stems from the singlet state.

3.4. Triplet State T_1 . The triplet state T_1 of the studied Cu(I) complexes is assigned as being of $^3(M+X)\text{LCT}$ character, which is based on DFT calculations (Figure 4). Additionally, the occurrence of only broad-band emission spectra even at low temperatures and of small $\Delta E(S_1-T_1)$ values supports this assignment. Literature classifications carried out for other Cu(I) complexes come to an equivalent characterization.^{23,37,41,43,44,51,82,86,93–97} The triplet state usually splits into three triplet substates. In organo-transition-metal com-

plexes, the corresponding splitting, the zero-field splitting (ZFS), is essentially determined by SOC to higher-lying singlet and triplet states.^{23–26,59,90,98–100} For emitting complexes, it is highly interesting to learn more about these substates. However, detailed studies are only rarely found. For example, theoretical investigations are reported in ref 23, while first experimental investigations have been carried out only recently.⁴¹ The reason why an experimental access to triplet substate properties of Cu(I) complexes is difficult is related to the occurrence of only very broad CT spectra (resulting from strong electron–phonon coupling⁹⁸) and thus to the difficulty of resolving the individual substates. Moreover, at temperatures higher than about 15–20 K, relaxation processes thermalize the population of the three substates in a time faster than that of the individual substate emission. Therefore, the information about the individual substate is lost. Accordingly, adequate investigations require measurements at very low temperature, that is, when fast processes of thermalization due to spin–lattice relaxation (SLR) are largely frozen out, at least for small $\Delta E(\text{ZFS})$ values.^{90,99–105} If so, individual substates can become observable.^{20–22,90,99–105} Hence, we extend our investigations of the triplet state properties down to $T = 1.3 \text{ K}$. Here, we focus on compound 1.

Figure 8 displays the emission decay behavior of compound 1. In the range of $15 < T < 300 \text{ K}$, the decay is

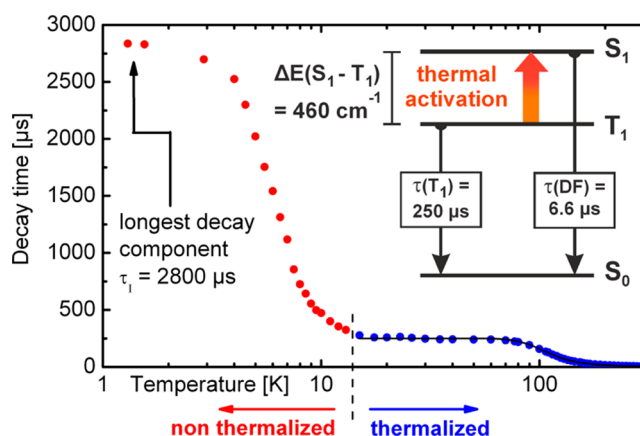


Figure 8. Emission decay time of compound 1 versus temperature. In the temperature range above $T \approx 15 \text{ K}$, the three triplet substates are in a fast thermal equilibrium, and only one decay component can be observed. At higher temperatures, $\sim 60 \text{ K}$, the singlet state S_1 becomes thermally populated, resulting in a reduction of the emission decay time. At ambient temperature, this process of TADF leads to a decay of $\tau(\text{DF}) = 6.6 \mu\text{s}$. In the inset, an energy level diagram of compound 1 is shown. With decreasing temperature below $T \approx 15 \text{ K}$, the emission decay deviates more and more from a single-exponential decay. In this part of the plot, only the longest decay component of the nonmonoexponential function is displayed (compare Figure 9).

monoexponential, and a very similar trend is observed as that for compound 3 (compare Figure 6). Fitting the measured data with eq 1 gives values of $\Delta E(S_1-T_1) = 460 \text{ cm}^{-1}$ and $\tau(S_1, \text{prompt}) = 210 \text{ ns}$ (inset of Figure 8). The decay time of the T_1 state, represented by the plateau, lies at $\tau(T_1) = 250 \mu\text{s}$. This value displays the emission decay time of all three triplet substates if thermally equilibrated (compare Figure 8 right-hand side). However, below $T \approx 15 \text{ K}$, the emission decay becomes more and more nonmonoexponential, and at $T = 1.3 \text{ K}$, the decay curve can be fitted well by three components with $\tau_I = 2.8 \text{ ms}$, $\tau_{II} = 1.0 \text{ ms}$, and $\tau_{III} = 90 \mu\text{s}$ (Figure 9). A similar three-

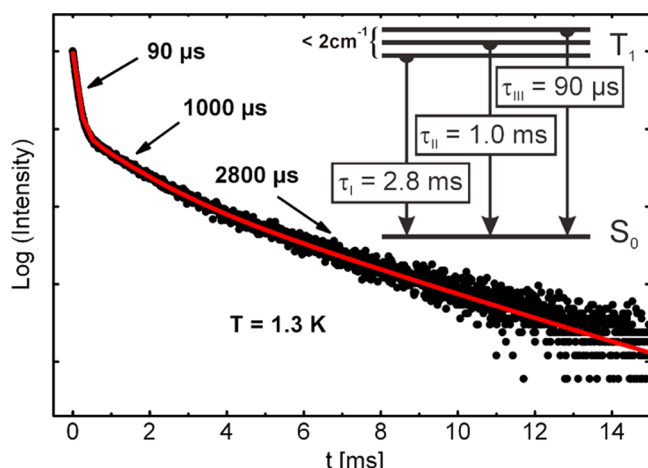


Figure 9. Emission decay behavior of compound **1** at $T = 1.3$ K. Pulsed excitation at $\lambda_{\text{exc}} = 355$ nm. The inset shows the triplet state T_1 with its substates I, II, and III and their respective individual decay times. The corresponding splitting is less than 2 cm^{-1} .

component decay has frequently been observed for other organo-transition-metal compounds, such as Pd(II) ,^{90,103} Pt(II) ,^{20,21,90} Ir(III) ,¹⁰¹ Re(I) ,¹⁰² and Cu(I) ⁴¹ complexes. The different decay components have been assigned to the emissions from the three individual triplet substates, which are zero-field split by less than 1 or 2 cm^{-1} and in several cases even much less.^{90,104} Such a behavior is a consequence of very slow SLR processes between energetically near-lying substates at very low temperature.¹⁰⁶ We apply an equivalent assignment also to the investigated Cu(I) compound and thus obtain the energy level diagram shown as the inset in Figure 9.

Obviously, the discussion presented above implies that below $T \approx 15$ K, eq 1 does not hold to describe the decay behavior (no thermalization). Nevertheless, in Figure 8, we extend the plot to temperatures below 15 K to visualize the drastic increase of the longest emission decay component. Interestingly, below $T \approx 3$ K, a second plateau is observed for this long component. It simply signifies that a further temperature decrease would not lead to any significant population change between the different substates.

In the case of a fast thermalization and for $\Delta E(\text{ZFS}) \ll k_B T$, the averaged decay time τ_{av} of the three substates can be expressed by the three individual decay times according to eq 6.^{90,105}

$$\tau_{\text{av}} = 3 \left[\frac{1}{\tau_I} + \frac{1}{\tau_{II}} + \frac{1}{\tau_{III}} \right]^{-1} \quad (6)$$

τ_I , τ_{II} , and τ_{III} represent the emission decay times of the individual triplet substates I, II, and III.

If the individual substate decay times as determined from the 1.3 K decay curve (Figure 9) are inserted, a value of $\tau_{\text{av}} = 241 \mu\text{s}$ is obtained. This value agrees well with the observed decay time of the plateau of $\tau(T_1) = 250 \mu\text{s}$. The pronounced correspondence substantiates that the three decay components determined at $T = 1.3$ K originate indeed from the triplet T_1 state.

Equivalent studies as discussed above have also been carried out for the compounds **2**, **3**, and **4** (Table 5). For example, the decay components of **3** were determined to be $\tau_I = 1.8 \text{ ms}$, $\tau_{II} = 630 \mu\text{s}$, and $\tau_{III} = 110 \mu\text{s}$. Using eq 6, this results in $\tau_{\text{av}} = 267 \mu\text{s}$. Within limits of experimental error of about 10%, also this value

Table 5. Emission Decay Times of the Triplet State T_1 and Its Respective Substates I, II, and III

compound	1	2	3	4	Ir(ppy)_3 ^a
$\tau_I [\mu\text{s}]$ ^b	2800	2200	1800	1500	116
$\tau_{II} [\mu\text{s}]$ ^b	1000	1100	630	500	6.6
$\tau_{III} [\mu\text{s}]$ ^b	90	850	110	110	0.2
$\tau_{\text{av}} [\mu\text{s}]$ calculated	241	1181	267	255	
$\tau(30 \text{ K}) [\mu\text{s}]$ measured	250	1200	300	270	

^aData from ref 18 for comparison. ^bThe error in the fit of the decay components is 10%.

fits well to the measured decay time in the range of the plateau with $\tau = 290 \mu\text{s}$. This holds similarly for the compounds **2** and **4**.

The individual decay components display some interesting trends. If we ignore nonradiative processes (at $T = 1.3$ K) for this discussion, we can use the reciprocal decay time as a measure of the allowedness or the radiative transition rate. Thus, it is seen that all transition rates are very small. This becomes apparent when the corresponding values are compared to those of the triplet substates of Ir(ppy)_3 , given in Table 5. In particular, the radiative rates of Ir(ppy)_3 are several orders of magnitude larger than those of the Cu(I) complexes. Obviously, this is a consequence of the effectiveness of SOC of the corresponding substates to higher-lying singlet states.^{18,23,24,26,110–113} Trends are also seen when the different copper complexes are compared. The decay time of substate I decreases in the series of **1** (Cl), **2** (Br), **3** (I), **4** (I) and thus displays some influence of the increasing SOC constant from Cl (SOC constant $\xi = 587 \text{ cm}^{-1}$), to Br (2460 cm^{-1}), to I (5069 cm^{-1}).⁵⁷ However, a corresponding trend does not occur for the decay times of substate III if **1** (Cl) is compared with **2** (Br), but these two compounds have different molecular structures (Figure 2). Apparently, the individual structure influences the effectiveness of SOC. Interestingly, the trend of increasing SOC induced by the halides is again observed (with respect to substate III) if **2** (Br) and **3** (I) are compared. Both compounds have similar molecular structures.

Interestingly, most organo-transition-metal compounds frequently exhibit orders of magnitude different emission decay times of the three triplet substates (compare the values given for Ir(ppy)_3 (Table 5) and many other compounds discussed in ref 26). This trend is also clearly seen for compounds **1**, **3**, and **4** but not for compound **2**. Obviously, for this compound, SOC of all three substates to higher-lying singlets is not very different. In this respect, compound **2** represents a very rare example. It is remarked that more detailed assignments concerning SOC paths would require theoretical calculations that include SOC. Such investigations have not been carried out for the studied compounds and only very rarely for other organo-transition-metal compounds.^{23,110–114}

A further aspect should be addressed. The lowest triplet states of the studied copper complexes have been assigned as $^3(\text{M+X})\text{LCT}$ states. According to Figure 4, the Cu(I) metal and halide atoms X are involved in the HOMO and, as discussed in section 3.2, also in the HOMO–1. Because, according to TDDFT calculations, transitions from these occupied MOs are involved in the properties of the lowest excited energy states, one would expect that the relatively heavy atoms with SOC constants⁵⁷ of $\xi(\text{Cu}) = 857 \text{ cm}^{-1}$ and $\xi(\text{I}) = 5069 \text{ cm}^{-1}$ for **3** and **4** would have a strong influence on the triplet state

properties such as large ZFSs and short decay times. However, this is not observed experimentally. Obviously, further investigations are required in this respect.

4. THERMALLY ACTIVATED DELAYED FLUORESCENCE, SINGLET HARVESTING, AND CONCLUDING REMARKS

Four new halide-bridged Cu(I) dimers with chelating amino-phosphane ligands were synthesized, structurally analyzed, and, in particular, photophysically characterized. At ambient temperature, the complexes exhibit high photoluminescence quantum yields (up to 65%) and relatively short emission decay times (down to about 4 μ s), and the emission color can be tuned from green to blue by variation of the halide X. The involved electronic transitions are assigned to (metal+halide)-to-ligand CT character. Accordingly, the lowest excited singlet (S_1) and triplet (T_1) states are designated as $^1,3(M+X)LCT$ states. With these transitions, a distinct CT is connected. Hence, the quantum mechanical exchange interaction and, thus, the resulting energy separations between the S_1 and the T_1 states $\Delta E(S_1-T_1)$ are expected to become relatively small. Indeed, the experimentally determined values amount only to a few hundred cm^{-1} (several 10 meV) and thus belong to the smallest energy separations reported for Cu(I) compounds so far. As a consequence, these materials are highly attractive candidates for studies and applications of TADF. For example, compound 3 ($[\text{Cu}(\mu\text{-I})(\text{PNMe}_2)_2]_2$), representing a blue light emitter ($\lambda_{\text{max}} = 464 \text{ nm}$, CIE coordinates (0.16; 0.22)) exhibits an activation energy of $\Delta E(S_1-T_1) = 570 \text{ cm}^{-1}$ (70 meV). According to the drastically higher allowedness of the $S_1 \rightarrow S_0$ transition with respect to the $T_1 \rightarrow S_0$ transition, the radiative path occurs via the S_1 state, if thermally activated. Thus, at ambient temperature, the observed emission stems almost completely from the S_1 state (98%). Only 2% results from the T_1 state. Consequently, the ambient temperature emission represents a fluorescence, though thermally activated from the long-lived triplet state reservoir. Hence, this emission is a $S_1 \rightarrow S_0$ delayed fluorescence. For compound 3, it decays with a time constant of $\tau(\text{DF}) = 4.6 \mu\text{s}$ (Figure 10). For completeness, it is remarked that a spontaneous fluorescence has not been observed. Obviously, this is a consequence of a down-ISC time from the S_1 to the T_1 state being significantly shorter than the spontaneous emission decay time of 90 ns as determined from a fit procedure. A spin-allowed transition corresponding to this fluorescence decay time is regarded as a moderately allowed one.¹¹⁵ Interestingly, an emitter showing efficient TADF is highly attractive for OLED applications because all singlet (25%) and all triplet (75%) excitons that are generated in the emitter layer and trapped by the emitter molecule can, at least in principle, be harvested.^{26,41,58,59,116} However, in contrast to the well-known triplet harvesting effect,^{1,7,26,28,29,59} harvesting according to the TADF mechanism occurs via the emitting singlet S_1 state (Figure 10). Therefore, the related mechanism has been designated as the singlet harvesting effect.^{26,41,58,59,116}

With respect to OLED applications, utilization of the singlet harvesting effect opens a new class of emitter materials. In particular, even emitter compounds with long-lived triplet state emissions, normally not applicable due to distinct roll-off effects (for example, by saturation effects), can be applied under the condition of occurrence of a thermally activated singlet state emission. As a consequence, OLED emitters based on expensive and rare iridium or platinum metals could, in the

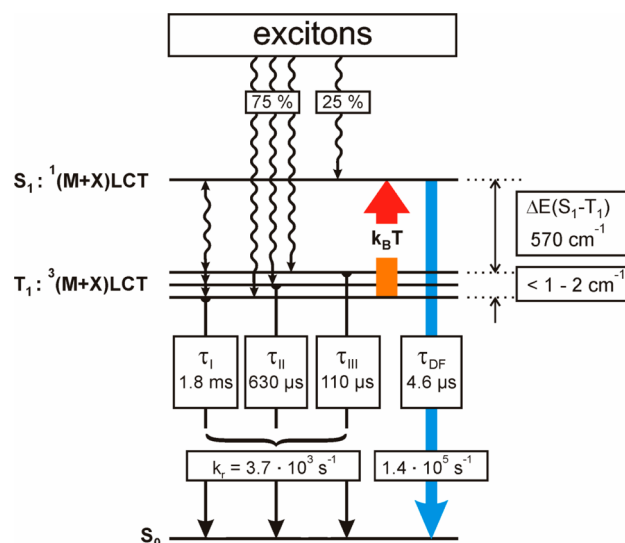


Figure 10. Energy level diagram and decay times for $[\text{Cu}(\mu\text{-I})(\text{PNMe}_2)_2]_2$ (compound 3). At a temperature below $T \approx 60 \text{ K}$, only a $T_1 \rightarrow S_0$ phosphorescence is observed. The T_1 state consists of three individual triplet substates I, II, and III. The corresponding decay times have been determined at $T = 1.3 \text{ K}$. The calculated averaged value corresponds well to the measured decay time of the triplet state T_1 of $\tau(T_1) = 290 \mu\text{s}$. The diagram displays also the (radiative) rates for the triplet state emission (calculated from the individual decay times as given in the diagram). With a temperature increase, the S_1 state is increasingly populated. As a consequence, the emission represents almost completely a TADF at ambient temperature with a decay time of $\tau(\text{DF}) = 6.6 \mu\text{s}$. This effect can be applied in an OLED device to harvest all excitons for an emission that stems from the singlet state, and hence, singlet harvesting becomes effective.

future, be replaced by complexes based on the abundant copper metal.^{26,39,41,49,51,58,59,117} Interestingly, even metal-free organic molecules, which exhibit efficient TADF,^{58,118–121} can be used to exploit the singlet harvesting effect in OLEDs.^{116,118–121} Indeed, efficient OLEDs based on the singlet harvesting mechanism have already been built.^{119,120,122} Interestingly, for the Cu(I) dimer 3, a short decay time of the delayed fluorescence, being of importance for reducing saturation effects, is already as short as $\tau(\text{DF}) = 4.6 \mu\text{s}$ with a radiative decay time of $\tau_r(\text{DF}) = 7.1 \mu\text{s}$. These $\tau(\text{DF})$ values are not yet as short as those found for the triplet emitter $\text{Ir}(\text{ppy})_3$ with $\tau(T_1) = 1.4 \mu\text{s}$ ($\tau_r(T_1) = 1.45 \mu\text{s}$),¹⁸ but they already approach the shortest-lived reported Pt(II)-based triplet emitters.²⁶ Further progress in developing shorter-lived TADF emitters is expected in the near future.

■ AUTHOR INFORMATION

Corresponding Authors

*E-mail: Hartmut.Yersin@ur.de (H.Y.).

*E-mail: Lars.Wesemann@uni-tuebingen.de (L.W.).

Notes

The authors declare no competing financial interest.

Crystallographic data (excluding structure factors) for the structures reported in this paper have been deposited with the Cambridge Crystallographic Data Centre as supplementary publication no. CCDC-929959 (1), CCDC-929960 (2), CCDC-929958 (3), and CCDC-929961 (4). Copies of the data can be obtained free of charge from www.ccdc.cam.ac.uk/conts/retrieving.html.

■ ACKNOWLEDGMENTS

We gratefully acknowledge the Bundesministerium für Bildung und Forschung (BMBF) for the funding of our research in the scope of the NEMO project (13N10619 and 13N10620).

■ REFERENCES

- (1) Yersin, H., Ed. *Highly Efficient OLEDs with Phosphorescent Materials*; Wiley-VCH: Weinheim, Germany, 2008.
- (2) Xiao, L.; Chen, Z.; Qu, B.; Luo, J.; Kong, S.; Gong, Q.; Kido, J. Recent Progresses on Materials for Electrophosphorescent Organic Light-Emitting Devices. *Adv. Mater.* **2011**, *23*, 926–952.
- (3) Brütting, W.; Adachi, C., Eds. *Physics of Organic Semiconductors*; Wiley-VCH: Weinheim, Germany, 2012.
- (4) Adachi, C.; Baldo, M. A.; Thompson, M. E.; Forrest, S. R. Nearly 100% Internal Phosphorescence Efficiency in an Organic Light-Emitting Device. *J. Appl. Phys.* **2001**, *90*, 5048–5051.
- (5) Kapturkiewicz, A. Electrochemiluminescent Systems as Devices and Sensors. *Electrochemistry of Functional Supramolecular Systems*; John Wiley & Sons, Inc.: New York, 2010; pp 477–522.
- (6) Costa, R. D.; Ortí, E.; Bolink, H. J. Recent Advances in Light-Emitting Electrochemical Cells. *Pure Appl. Chem.* **2011**, *83*, 2115–2128.
- (7) Baldo, M. A.; Lamansky, S.; Burrows, P. E.; Thompson, M. E.; Forrest, S. R. Very High-Efficiency Green Organic Light-Emitting Devices Based on Electrophosphorescence. *Appl. Phys. Lett.* **1999**, *75*, 4–6.
- (8) Tan, G.; Chen, S.; Sun, N.; Li, Y.; Fortin, D.; Wong, W.-Y.; Kwok, H.-S.; Ma, D.; Wu, H.; Wang, L.; et al. Highly Efficient Iridium(III) Phosphors with Phenoxy-Substituted Ligands and Their High-Performance OLEDs. *J. Mater. Chem. C* **2013**, *1*, 808.
- (9) Hanson, K.; Tamayo, A.; Diev, V. V.; Whited, M. T.; Djurovich, P. I.; Thompson, M. E. Efficient Dipyrrin-Centered Phosphorescence at Room Temperature from Bis-Cyclometalated Iridium(III) Dipyrrinato Complexes. *Inorg. Chem.* **2010**, *49*, 6077–6084.
- (10) Chen, H.-F.; Wu, C.; Kuo, M.-C.; Thompson, M. E.; Wong, K.-T. Anionic Iridium Complexes for Solid State Light-Emitting Electrochemical Cells. *J. Mater. Chem.* **2012**, *22*, 9556–9561.
- (11) Borek, C.; Hanson, K.; Djurovich, P. I.; Thompson, M. E.; Aznavour, K.; Bau, R.; Sun, Y.; Forrest, S. R.; Brooks, J.; Michalski, L.; et al. Highly Efficient, Near-Infrared Electrophosphorescence from a Pt-Metalloporphyrin Complex. *Angew. Chem., Int. Ed.* **2007**, *46*, 1109–1112.
- (12) Hudson, Z. M.; Sun, C.; Helander, M. G.; Chang, Y.-L.; Lu, Z.-H.; Wang, S. Highly Efficient Blue Phosphorescence from Triarylboron-Functionalized Platinum(II) Complexes of N-Heterocyclic Carbenes. *J. Am. Chem. Soc.* **2012**, *134*, 13930–13933.
- (13) Kui, S. C. F.; Chow, P. K.; Cheng, G.; Kwok, C.-C.; Kwong, C. L.; Low, K.-H.; Che, C.-M. Robust Phosphorescent Platinum(II) Complexes with Tetradentate O^NC^NC^N Ligands: High Efficiency OLEDs with Excellent Efficiency Stability. *Chem. Commun.* **2013**, *49*, 1497–1499.
- (14) Rossi, E.; Colombo, A.; Dragonetti, C.; Roberto, D.; Ugo, R.; Valore, A.; Falciola, L.; Brulatti, P.; Cocchi, M.; Williams, J. A. G. Novel N^CC^N-Cyclometallated Platinum Complexes with Acetylide Co-Ligands as Efficient Phosphors for OLEDs. *J. Mater. Chem.* **2012**, *22*, 10650–10655.
- (15) Murphy, L.; Brulatti, P.; Fattori, V.; Cocchi, M.; Williams, J. A. G. Blue-Shifting the Monomer and Excimer Phosphorescence of Tridentate Cyclometallated Platinum(II) Complexes for Optimal White-Light OLEDs. *Chem. Commun.* **2012**, *48*, 5817–5819.
- (16) Che, C.-M.; Kwok, C.-C.; Lai, S.-W.; Rausch, A. F.; Finkenzeller, W. J.; Zhu, N.; Yersin, H. Photophysical Properties and OLED Applications of Phosphorescent Platinum(II) Schiff Base Complexes. *Chem.—Eur. J.* **2010**, *16*, 233–247.
- (17) Finkenzeller, W. J.; Hofbeck, T.; Thompson, M. E.; Yersin, H. Triplet State Properties of the OLED Emitter Ir(btp)₂(acac): Characterization by Site-Selective Spectroscopy and Application of High Magnetic Fields. *Inorg. Chem.* **2007**, *46*, 5076–5083.
- (18) Hofbeck, T.; Yersin, H. The Triplet State of fac-Ir(ppy)₃. *Inorg. Chem.* **2010**, *49*, 9290–9299.
- (19) Brooks, J.; Babayan, Y.; Lamansky, S.; Djurovich, P. I.; Tsyba, I.; Bau, R.; Thompson, M. E. Synthesis and Characterization of Phosphorescent Cyclometalated Platinum Complexes. *Inorg. Chem.* **2002**, *41*, 3055–3066.
- (20) Fischer, T.; Czerwieniec, R.; Hofbeck, T.; Osmolina, M. M.; Yersin, H. Triplet State Properties of a Red Light Emitting [Pt(s-thpy)(acac)] Compound. *Chem. Phys. Lett.* **2010**, *486*, 53–59.
- (21) Rausch, A. F.; Monkowius, U. V.; Zabel, M.; Yersin, H. Bright Sky-Blue Phosphorescence of [*n*-Bu₄N][Pt(4,6-dFppy)(CN)₂]: Synthesis, Crystal Structure, and Detailed Photophysical Studies. *Inorg. Chem.* **2010**, *49*, 7818–7825.
- (22) Rausch, A. F.; Thompson, M. E.; Yersin, H. Matrix Effects on the Triplet State of the OLED Emitter Ir(4,6-dFppy)₂(pic) (FIrpic): Investigations by High-Resolution Optical Spectroscopy. *Inorg. Chem.* **2009**, *48*, 1928–1937.
- (23) Siddique, Z. A.; Yamamoto, Y.; Ohno, T.; Nozaki, K. Structure-Dependent Photophysical Properties of Singlet and Triplet Metal-to-Ligand Charge Transfer States in Copper(I) Bis(diimine) Compounds. *Inorg. Chem.* **2003**, *42*, 6366–6378.
- (24) Rausch, A. F.; Homeier, H. H. H.; Yersin, H. Organometallic Pt(II) and Ir(III) Triplet Emitters for OLED Applications and the Role of Spin–Orbit Coupling: A Study Based on High-Resolution Optical Spectroscopy. *Top. Organomet. Chem.* **2010**, *29*, 193–235.
- (25) Rausch, A. F.; Homeier, H. H. H.; Djurovich, P. I.; Thompson, M. E.; Yersin, H. Spin–Orbit Coupling Routes and OLED Performance — Studies of Blue Light Emitting Ir(III) and Pt(II) Complexes. In *Organic Light Emitting Materials and Devices XI*; Kafafi, Z. H., So, F., Eds.; SPIE: Bellingham, WA, 2007; Vol. 6655, pp 66550F-1.
- (26) Yersin, H.; Rausch, A. F.; Czerwieniec, R.; Hofbeck, T.; Fischer, T. The Triplet State of Organo-Transition Metal Compounds. Triplet Harvesting and Singlet Harvesting for Efficient OLEDs. *Coord. Chem. Rev.* **2011**, *255*, 2622–2652.
- (27) Kawamura, Y.; Goushi, K.; Brooks, J.; Brown, J. J.; Sasabe, H.; Adachi, C. 100% Phosphorescence Quantum Efficiency of Ir(III) Complexes in Organic Semiconductor Films. *Appl. Phys. Lett.* **2005**, *86*, 071104.
- (28) Baldo, M. A.; O'Brien, D. F.; You, Y.; Shoustikov, A.; Sibley, S.; Thompson, M. E.; Forrest, S. R. Highly Efficient Phosphorescent Emission from Organic Electroluminescent Devices. *Nature* **1998**, *395*, 151–154.
- (29) Yersin, H. Triplet Emitters for OLED Applications. Mechanisms of Exciton Trapping and Control of Emission Properties. *Top. Curr. Chem.* **2004**, *241*, 1–26.
- (30) Helfrich, W.; Schneider, W. G. Transients of Volume-Controlled Current and of Recombination Radiation in Anthracene. *J. Chem. Phys.* **1966**, *44*, 2902–2909.
- (31) Ford, P. C.; Cariati, E.; Bourassa, J. Photoluminescence Properties of Multinuclear Copper(I) Compounds. *Chem. Rev.* **1999**, *99*, 3625–3648.
- (32) Hardt, H. D.; Gechnizdjani, H. Fluoreszenz-Thermochrome Verbindungen von Kupfer(I)-jodid mit Äthyl- und Aminopyridinen. *Z. Anorg. Allg. Chem.* **1973**, *397*, 23–30.
- (33) Hardt, H. D.; Pierre, A. Fluorescence Thermochromism of Pyridine Copper Iodides and Copper Iodide. *Z. Anorg. Allg. Chem.* **1973**, *402*, 107–112.
- (34) Yam, V. W.-W.; Lo, K. K.-W.; Fung, W. K.-M.; Wang, C.-R. Design of Luminescent Polynuclear Copper(I) and Silver(I) Complexes with Chalcogenides and Acetylides as the Bridging Ligands. *Coord. Chem. Rev.* **1998**, *171*, 17–41.
- (35) Ford, P. C.; Vogler, A. Photochemical and Photophysical Properties of Tetranuclear and Hexanuclear Clusters of Metals with d¹⁰ and s² Electronic Configurations. *Acc. Chem. Res.* **1993**, *26*, 220–226.
- (36) Kutal, C. Spectroscopic and Photochemical Properties of d¹⁰ Metal Complexes. *Coord. Chem. Rev.* **1990**, *99*, 213–252.

- (37) Blasse, G.; McMillin, D. R. On the Luminescence of Bis(Triphenylphosphine) Phenanthroline Copper(I). *Chem. Phys. Lett.* **1980**, *70*, 1–3.
- (38) Liu, Z.; Djurovich, P. I.; Whited, M. T.; Thompson, M. E. Cu₄I₄ Clusters Supported by P⁺N-Type Ligands: New Structures with Tunable Emission Colors. *Inorg. Chem.* **2012**, *51*, 230–236.
- (39) Hashimoto, M.; Igawa, S.; Yashima, M.; Kawata, I.; Hoshino, M.; Osawa, M. Highly Efficient Green Organic Light-Emitting Diodes Containing Luminescent Three-Coordinate Copper(I) Complexes. *J. Am. Chem. Soc.* **2011**, *133*, 10348–10351.
- (40) Lotito, K. J.; Peters, J. C. Efficient Luminescence from Easily Prepared Three-Coordinate Copper(I) Arylamidophosphines. *Chem. Commun.* **2010**, *46*, 3690–3692.
- (41) Czerwieniec, R.; Yu, J.; Yersin, H. Blue-Light Emission of Cu(I) Complexes and Singlet Harvesting. *Inorg. Chem.* **2011**, *50*, 8293–8301.
- (42) Miller, A. J. M.; Dempsey, J. L.; Peters, J. C. Long-Lived and Efficient Emission from Mononuclear Amidophosphine Complexes of Copper. *Inorg. Chem.* **2007**, *46*, 7244–7246.
- (43) Tsuboyama, A.; Kuge, K.; Furugori, M.; Okada, S.; Hoshino, M.; Ueno, K. Photophysical Properties of Highly Luminescent Copper(I) Halide Complexes Chelated with 1,2-Bis(diphenylphosphino)benzene. *Inorg. Chem.* **2007**, *46*, 1992–2001.
- (44) Moudam, O.; Kaeser, A.; Delavaux-Nicot, B.; Duhayon, C.; Holler, M.; Accorsi, G.; Armaroli, N.; Seguy, I.; Navarro, J.; Destruel, P.; et al. Electrophosphorescent Homo- and Heteroleptic Copper(I) Complexes Prepared from Various Bis-Phosphine Ligands. *Chem. Commun.* **2007**, 3077–3079.
- (45) McCormick, T.; Jia, W.-L.; Wang, S. Phosphorescent Cu(I) Complexes of 2-(2'-Pyridylbenzimidazolyl)benzene: Impact of Phosphine Ancillary Ligands on Electronic and Photophysical Properties of the Cu(I) Complexes. *Inorg. Chem.* **2006**, *45*, 147–155.
- (46) Qin, L.; Zhang, Q.; Sun, W.; Wang, J.; Lu, C.; Cheng, Y.; Wang, L. Novel Luminescent Iminophosphine Complex of Copper(I) with High Photochemical and Electrochemical Stability. *Dalton Trans.* **2009**, 9388–9391.
- (47) Harkins, S. B.; Peters, J. C. A Highly Emissive Cu₂N₂ Diamond Core Complex Supported by a [PNP][−] Ligand. *J. Am. Chem. Soc.* **2005**, *127*, 2030–2031.
- (48) Mankad, N. P.; Rivard, E.; Harkins, S. B.; Peters, J. C. Structural Snapshots of a Flexible Cu₂P₂ Core that Accommodates the Oxidation States Cu^ICu^I, Cu^{I.5}Cu^{1.5}, and Cu^{II}Cu^{II}. *J. Am. Chem. Soc.* **2005**, *127*, 16032–16033.
- (49) Deaton, J. C.; Switalski, S. C.; Kondakov, D. Y.; Young, R. H.; Pawlik, T. D.; Giesen, D. J.; Harkins, S. B.; Miller, A. J. M.; Mickenberg, S. F.; Peters, J. C. E-Type Delayed Fluorescence of a Phosphine-Supported Cu₂(μ-NAr₂)₂ Diamond Core: Harvesting Singlet and Triplet Excitons in OLEDs. *J. Am. Chem. Soc.* **2010**, *132*, 9499–9508.
- (50) Liu, X.; Sun, W.; Zou, L.; Xie, Z.; Li, X.; Lu, C.; Wang, L.; Cheng, Y. Neutral Cuprous Complexes as Ratiometric Oxygen Gas Sensors. *Dalton Trans.* **2012**, *41*, 1312–1319.
- (51) Zink, D. M.; Bächle, M.; Baumann, T.; Nieger, M.; Kuhn, M.; Wang, C.; Kloppe, W.; Monkowius, U.; Hofbeck, T.; Yersin, H.; et al. Synthesis, Structure, and Characterization of Dinuclear Copper(I) Halide Complexes with P⁺N Ligands Featuring Exciting Photoluminescence Properties. *Inorg. Chem.* **2013**, *52*, 2292–2305.
- (52) Chiarella, G.; Melgarejo, D.; Fackler, J. P., Jr. Synthesis, Characterization and Properties of a Novel Cationic Hexanuclear Cyclic Guanidinate Copper(I) Cluster of High Solubility in Non-polar Solvents. *J. Cluster Sci.* **2012**, *23*, 823–838.
- (53) Czerwieniec, R.; Kowalski, K.; Yersin, H. Highly Efficient Thermally Activated Fluorescence of a New Rigid Cu(I) Complex [Cu(dmp)(phanephos)]⁺. *Dalton Trans.* **2013**, *42*, 9826–9830.
- (54) Baldo, M. A.; Adachi, C.; Forrest, S. R. Transient Analysis of Organic Electrophosphorescence. II. Transient Analysis of Triplet–Triplet Annihilation. *Phys. Rev. B* **2000**, *62*, 10967–10977.
- (55) Giebink, N. C.; Forrest, S. R. Quantum Efficiency Roll-Off at High Brightness in Fluorescent and Phosphorescent Organic Light Emitting Diodes. *Phys. Rev. B* **2008**, *77*, 235215.
- (56) Tanaka, D.; Sasabe, H.; Li, Y.-J.; Su, S.-J.; Takeda, T.; Kido, J. Ultra High Efficiency Green Organic Light-Emitting Devices. *Jpn. J. Appl. Phys.* **2007**, *46*, L10.
- (57) Murov, S. L.; Hug, G. L.; Carmichael, I. *Handbook of Photochemistry*, 2nd ed.; Marcel Dekker: New York, 1993; pp 339–341.
- (58) Yersin, H.; Czerwieniec, R.; Hupfer, A. Singlet Harvesting with Brightly Emitting Cu(I) and Metal-Free Organic Compounds. *Proc. SPIE* **2012**, 843508–843508.
- (59) Yersin, H.; Rausch, A. F.; Czerwieniec, R. Organometallic Emitters for OLEDs: Triplet Harvesting, Singlet Harvesting, Case Structures, and Trends. *Physics of Organic Semiconductors*; Wiley-VCH Verlag: New York, 2012; pp 371–424.
- (60) Fritz, H. P.; Gordon, I. R.; Schwarzthans, K. E.; Venanzi, L. M. Some Complexes of Palladium(II) and Platinum(II) with Mixed Phosphorus-Nitrogen Ligands. *J. Chem. Soc.* **1965**, 5210–5216.
- (61) X-Area 1.26; Stoe & Cie GmbH: Darmstadt, Germany, 2004.
- (62) Sheldrick, G. M. *SHELXS 97*; University of Göttingen: Göttingen, Germany, 1997.
- (63) X-SHAPE 2.05; Stoe & Cie GmbH: Darmstadt, Germany, 2004.
- (64) Valiev, M.; Bylaska, E. J.; Govind, N.; Kowalski, K.; Straatsma, T. P.; Van Dam, H. J. J.; Wang, D.; Nieplocha, J.; Apra, E.; Windus, T. L.; et al. NWChem: A Comprehensive and Scalable Open-Source Solution for Large Scale Molecular Simulations. *Comput. Phys. Commun.* **2010**, *181*, 1477–1489.
- (65) Becke, A. D. Density-Functional Thermochemistry. III. The Role of Exact Exchange. *J. Chem. Phys.* **1993**, *98*, 5648.
- (66) Dill, J. D.; Pople, J. A. Self-Consistent Molecular Orbital Methods. XV. Extended Gaussian-Type Basis Sets for Lithium, Beryllium, and Boron. *J. Chem. Phys.* **1975**, *62*, 2921–2923.
- (67) Franci, M. M.; Pietro, W. J.; Hehre, W. J.; Binkley, J. S.; Gordon, M. S.; DeFrees, D. J.; Pople, J. A. Self-Consistent Molecular Orbital Methods. XXIII. A Polarization-Type Basis Set for Second-Row Elements. *J. Chem. Phys.* **1982**, *77*, 3654–3665.
- (68) Hehre, W. J.; Ditchfield, R.; Pople, J. A. Self-Consistent Molecular Orbital Methods. XII. Further Extensions of Gaussian-Type Basis Sets for Use in Molecular Orbital Studies of Organic Molecules. *J. Chem. Phys.* **1972**, *56*, 2257–2261.
- (69) Rassolov, V. A.; Pople, J. A.; Ratner, M. A.; Windus, T. L. 6-31G(*) Basis Set for Atoms K through Zn. *J. Chem. Phys.* **1998**, *109*, 1223–1229.
- (70) Mitin, A. V.; Baker, J.; Pulay, P. An Improved 6-31G(*) Basis Set for First-Row Transition Metals. *J. Chem. Phys.* **2003**, *118*, 7775–7782.
- (71) Dunning, T. H.; Hay, P. J. *Methods of Electronic Structure Theory*; Plenum: New York, 1977; Vol. 2.
- (72) Hay, P. J.; Wadt, W. R. Ab Initio Effective Core Potentials for Molecular Calculations. Potentials for the Transition Metal Atoms Sc to Hg. *J. Chem. Phys.* **1985**, *82*, 270–283.
- (73) Hay, P. J.; Wadt, W. R. Ab Initio Effective Core Potentials for Molecular Calculations. Potentials for K to Au Including the Outermost Core Orbitals. *J. Chem. Phys.* **1985**, *82*, 299–310.
- (74) Wadt, W. R.; Hay, P. J. Ab Initio Effective Core Potentials for Molecular Calculations. Potentials for Main Group Elements Na to Bi. *J. Chem. Phys.* **1985**, *82*, 284–298.
- (75) Dyason, J. C.; Engelhardt, L. M.; Healy, P. C.; Pakawatchai, C.; White, A. H. Lewis Base Adducts of Group 11 Metal Compounds. 14. Crystal Structures of the 1:2 Binuclear Adducts of Copper(I) Halides with some 2(4)-Mono- and Dimethyl-Substituted Pyridine Bases and Quinoline. *Inorg. Chem.* **1985**, *24*, 1950–1957.
- (76) Oakley, S. H.; Soria, D. B.; Coles, M. P.; Hitchcock, P. B. Structural Diversity in the Coordination of Amidines and Guanidines to Monovalent Metal Halides. *Dalton Trans.* **2004**, 537–546.
- (77) Oshio, H.; Watanabe, T.; Ohto, A.; Ito, T.; Masuda, H. Intermolecular Ferromagnetic and Antiferromagnetic Interactions in Halogen-Bridged Copper(I) Imino Nitroxides: Crystal Structures and Magnetic Properties of [CuI(μ-X)(imino nitroxide)]₂ (X = I or Br). *Inorg. Chem.* **1996**, *35*, 472–479.

- (78) Toth, A.; Floriani, C.; Chiesi-Villa, A.; Guastini, C. Copper(I)–Benzimidazole Adducts: From Mononuclear to Polymeric Complexes. *Inorg. Chem.* **1987**, *26*, 3897–3902.
- (79) Fu, W.-F.; Gan, X.; Che, C.-M.; Cao, Q.-Y.; Zhou, Z.-Y.; Zhu, N. N.-Y. Cuprophilic Interactions in Luminescent Copper(I) Clusters with Bridging Bis(dicyclohexylphosphino)methane and Iodide Ligands: Spectroscopic and Structural Investigations. *Chem.—Eur. J.* **2004**, *10*, 2228–2236.
- (80) Chesnut, D. J.; Kusnetzow, A.; Birge, R. R.; Zubieta, J. Solid State Coordination Chemistry of the Copper Halide- and Pseudo-Halide-Organamine System, Cu-X-[(bis-2,3-(2-pyridyl)pyrazine)] (X = Cl, Br, CN): Hydrothermal Synthesis and Structural Characterization. *Inorg. Chem.* **1999**, *38*, 2663–2671.
- (81) Dexter, D. L.; Schulman, J. H. Theory of Concentration Quenching in Inorganic Phosphors. *J. Chem. Phys.* **1954**, *22*, 1063–1070.
- (82) Felder, D.; Nierengarten, J.-F.; Barigelletti, F.; Ventura, B.; Armaroli, N. Highly Luminescent Cu(I)–Phenanthroline Complexes in Rigid Matrix and Temperature Dependence of the Photophysical Properties. *J. Am. Chem. Soc.* **2001**, *123*, 6291–6299.
- (83) Vorontsov, I. I.; Graber, T.; Kovalevsky, A. Y.; Novozhilova, I. V.; Gembicky, M.; Chen, Y.-S.; Coppens, P. Capturing and Analyzing the Excited-State Structure of a Cu(I) Phenanthroline Complex by Time-Resolved Diffraction and Theoretical Calculations. *J. Am. Chem. Soc.* **2009**, *131*, 6566–6573.
- (84) Shaw, G. B.; Grant, C. D.; Shiota, H.; Castner, E. W.; Meyer, G. J.; Chen, L. X. Ultrafast Structural Rearrangements in the MLCT Excited State for Copper(I) bis-Phenanthrolines in Solution. *J. Am. Chem. Soc.* **2007**, *129*, 2147–2160.
- (85) Sakaki, S.; Mizutani, H.; Kase, Y. Geometry, Electronic Structure, and Coordination Ability of $[\text{Cu}(\text{diN})(\text{PH}_3)_2]^+$ (diN = HN=CHCH=NH) at the Lowest Energy Triplet Metal-to-Ligand Charge-Transfer Excited State. A Theoretical Study. *Inorg. Chem.* **1992**, *31*, 4575–4581.
- (86) Cunningham, C. T.; Moore, J. J.; Cunningham, K. L. H.; Fanwick, P. E.; McMillin, D. R. Structural and Photophysical Studies of $\text{Cu}(\text{NN})_2^+$ Systems in the Solid State. Emission at Last from Complexes with Simple 1,10-Phenanthroline Ligands. *Inorg. Chem.* **2000**, *39*, 3638–3644.
- (87) Rössler, U.; Yersin, H. Destabilization of a Self-Trapped Exciton in a Quasi-One-Dimensional Semiconductor: $\text{Mg}[\text{Pt}(\text{CN})_4] \cdot 7\text{H}_2\text{O}$ with Hydrostatic Pressure. *Phys. Rev. B* **1982**, *26*, 3187–3191.
- (88) Azumi, T.; O'Donnell, C. M.; McGlynn, S. P. On the Multiplicity of the Phosphorescent State of Organic Molecules. *J. Chem. Phys.* **1966**, *45*, 2735–2742.
- (89) Harrigan, R. W.; Crosby, G. A. Symmetry Assignments of the Lowest CT Excited States of Ruthenium (II) Complexes via a Proposed Electronic Coupling Model. *J. Chem. Phys.* **1973**, *59*, 3468–3476.
- (90) Yersin, H.; Donges, D. Low-Lying Electronic States and Photophysical Properties of Organometallic Pd(II) and Pt(II) Compounds. Modern Research Trends Presented in Detailed Case Studies. *Top. Curr. Chem.* **2001**, *214*, 81–186.
- (91) Hill, M. G.; Bailey, J. A.; Miskowski, V. M.; Gray, H. B. Spectroelectrochemistry and Dimerization Equilibria of Chloro-(terpyridine)platinum(II). Nature of the Reduced Complexes. *Inorg. Chem.* **1996**, *35*, 4585–4590.
- (92) Atkins, P. W.; Friedman, R. S. *Molecular Quantum Mechanics*; Oxford University Press: Oxford, U.K., 2010.
- (93) Chen, J.-L.; Cao, X.-F.; Gu, W.; Su, B.-T.; Zhang, F.; Wen, H.-R.; Hong, R. Luminescent Mononuclear Copper(I) Heteroleptic Complexes with 6-Cyano-2,2'-bipyridine. *Inorg. Chem. Commun.* **2012**, *15*, 65–68.
- (94) Hsu, C.-W.; Lin, C.-C.; Chung, M.-W.; Chi, Y.; Lee, G.-H.; Chou, P.-T.; Chang, C.-H.; Chen, P.-Y. Systematic Investigation of the Metal-Structure–Photophysics Relationship of Emissive d^{10} -Complexes of Group 11 Elements: The Prospect of Application in Organic Light Emitting Devices. *J. Am. Chem. Soc.* **2011**, *133*, 12085–12099.
- (95) Krylova, V. A.; Djurovich, P. I.; Aronson, J. W.; Haiges, R.; Whited, M. T.; Thompson, M. E. Structural and Photophysical Studies of Phosphorescent Three-Coordinate Copper(I) Complexes Supported by an N-Heterocyclic Carbene Ligand. *Organometallics* **2012**, *31*, 7983–7993.
- (96) Krylova, V. A.; Djurovich, P. I.; Whited, M. T.; Thompson, M. E. Synthesis and Characterization of Phosphorescent Three-Coordinate Cu(I)–NHC Complexes. *Chem. Commun.* **2010**, *46*, 6696–6698.
- (97) McMillin, D. R.; McNett, K. M. Photoprocesses of Copper Complexes That Bind to DNA. *Chem. Rev.* **1998**, *98*, 1201–1220.
- (98) Yersin, H.; Finkenzeller, W. J. Triplet Emitters for Organic Light-Emitting Diodes: Basic Properties. In *Highly Efficient OLEDs with Phosphorescent Materials*; Wiley-VCH Verlag GmbH & Co. KGaA: New York, 2008; pp 1–97.
- (99) Yersin, H.; Strasser, J. Triplets in Metal–Organic Compounds. Chemical Tunability of Relaxation Dynamics. *Coord. Chem. Rev.* **2000**, *208*, 331–364.
- (100) Rausch, A. F.; Thompson, M. E.; Yersin, H. Triplet State Relaxation Processes of the OLED Emitter $\text{Pt}(4,6\text{-dFppy})(\text{acac})$. *Chem. Phys. Lett.* **2009**, *468*, 46–51.
- (101) Finkenzeller, W. J.; Stöfel, P.; Yersin, H. Emission and Absorption of $\text{Ir}(\text{ppy})_2(\text{CO})(\text{Cl})$ — Temperature Dependence, Phosphorescence Decay Dynamics, and Assignment of Excited States. *Chem. Phys. Lett.* **2004**, *397*, 289–295.
- (102) Czerwieniec, R.; Finkenzeller, W. J.; Hofbeck, T.; Starukhin, A.; Wedel, A.; Yersin, H. Photophysical Properties of $\text{Re}(\text{pbt})(\text{CO})_4$ Studied by High Resolution Spectroscopy. *Chem. Phys. Lett.* **2009**, *468*, 205–210.
- (103) Schmidt, J.; Wiedenhofer, H.; von Zelewsky, A.; Yersin, H. Time-Resolved Vibrational Structures of the Triplet Sublevel Emission of $\text{Pd}(\text{2-thpy})_2$. *J. Phys. Chem.* **1995**, *99*, 226–229.
- (104) Yersin, H.; Donges, D.; Nagle, J. K.; Sitters, R.; Glasbeek, M. Intraligand Charge Transfer in the Pd(II) Oxinate Complex $\text{Pd}(\text{qol})_2$. Site-Selective Emission, Excitation, and Optically Detected Magnetic Resonance. *Inorg. Chem.* **2000**, *39*, 770–777.
- (105) Tinti, D. S.; El-Sayed, M. A. New Techniques in Triplet State Phosphorescence Spectroscopy: Application to the Emission of 2,3-Dichloroquinoxaline. *J. Chem. Phys.* **1971**, *54*, 2529–2549.
- (106) An occurrence of a distinctly larger energy separation $\Delta E(\text{ZFS})$ between the triplet substates is not probable because already a splitting of a few cm^{-1} would induce decay components of less than a few μs according to fast spin–lattice relaxation processes even at $T = 1.3\text{ K}$ (refs 99, 107–109). However, correspondingly short decay components have not been observed.
- (107) Abragam, A.; Bleaney, B. *Electron Paramagnetic Resonance of Transition Ions*; Clarendon Press: Oxford, U.K., 1970.
- (108) Henderson, B.; Imbusch, G. F. *Optical Spectroscopy of Inorganic Solids*; Clarendon Press: Oxford, U.K., 1989.
- (109) Manenkov, A. A.; Orbach, R. *Spin-Lattice Relaxation in Ionic Solids*; Harper & Row: New York, 1966.
- (110) Nozaki, K. Theoretical Studies on Photophysical Properties and Mechanism of Phosphorescence in $[\text{fac-Ir}(\text{2-phenylpyridine})_3]$. *J. Chin. Chem. Soc. (Taipei, Taiwan)* **2006**, *53*, 101.
- (111) Obara, S.; Itabashi, M.; Okuda, F.; Tamaki, S.; Tanabe, Y.; Ishii, Y.; Nozaki, K.; Haga, M. A. Highly Phosphorescent Iridium Complexes Containing Both Tridentate Bis(benzimidazolyl)-benzene or -pyridine and Bidentate Phenylpyridine: Synthesis, Photophysical Properties, and Theoretical Study of Ir–Bis(benzimidazolyl)benzene Complex. *Inorg. Chem.* **2006**, *45*, 8907–8921.
- (112) Jansson, E.; Minaev, B.; Schrader, S.; Ågren, H. Time-Dependent Density Functional Calculations of Phosphorescence Parameters for fac-tris(2-phenylpyridine) Iridium. *Chem. Phys.* **2007**, *333*, 157–167.
- (113) Jacko, A. C.; McKenzie, R. H.; Powell, B. J. Models of Organometallic Complexes for Optoelectronic Applications. *J. Mater. Chem.* **2010**, *20*, 10301–10307.

- (114) Li, X.; Minaev, B.; Ågren, H.; Tian, H. Theoretical Study of Phosphorescence of Iridium Complexes with Fluorine-Substituted Phenylpyridine Ligands. *Eur. J. Inorg. Chem.* **2011**, 2011, 2517–2524.
- (115) Turro, N. J. *Modern Molecular Chemistry*; Benjamin/Cummings Publishing Company, Inc.: Menlo Park, CA, 1978.
- (116) Yersin, H.; Monkowius, U. Singlet Harvesting, DE 10 2008 033 563 A1, Internal filing University of Regensburg, August, 2006.
- (117) Igawa, S.; Hashimoto, M.; Kawata, I.; Yashima, M.; Hoshino, M.; Osawa, M. Highly Efficient Green Organic Light-Emitting Diodes Containing Luminescent Tetrahedral Copper(I) Complexes. *J. Mater. Chem. C* **2013**, 1, 542–551.
- (118) Tanaka, H.; Shizu, K.; Miyazaki, H.; Adachi, C. Efficient Green Thermally Activated Delayed Fluorescence (TADF) from a Phenoxazine-Triphenyltriazine (PXZ-TRZ) Derivative. *Chem. Commun.* **2012**, 48, 11392–11394.
- (119) Uoyama, H.; Goushi, K.; Shizu, K.; Nomura, H.; Adachi, C. Highly Efficient Organic Light-Emitting Diodes from Delayed Fluorescence. *Nature* **2012**, 492, 234–238.
- (120) Zhang, Q.; Li, J.; Shizu, K.; Huang, S.; Hirata, S.; Miyazaki, H.; Adachi, C. Design of Efficient Thermally Activated Delayed Fluorescence Materials for Pure Blue Organic Light Emitting Diodes. *J. Am. Chem. Soc.* **2012**, 134, 14706–14709.
- (121) Yersin, H. WO 2012/001002 A2, June, 2010.
- (122) Nakagawa, T.; Ku, S.-Y.; Wong, K.-T.; Adachi, C. Electroluminescence Based on Thermally Activated Delayed Fluorescence Generated by a Spirobifluorene Donor–Acceptor Structure. *Chem. Commun.* **2012**, 48, 9580–9582.